

ALPHA FOUNDATION FOR THE IMPROVEMENT OF MINE SAFETY AND HEALTH

Final Technical Report

Project Title	Exploration of Temporal Changes in Respirable Coal Mine Dust Characteristics
Grant Number	AFCTG20-104
Organization	Virginia Polytechnic Institute and State University
Principal Investigator	Emily Sarver
Co-Principal Investigator	Cigdem Keles
Contact Information	Email: esarver@vt.edu Phone: 540-231-8139 Fax: 540-231-4070
Period of Performance:	Jan 1, 2021 – Dec 31, 2022

Acknowledgement/Disclaimer: This study was sponsored by the Alpha Foundation for the Improvement of Mine Safety and Health, Inc. (ALPHA FOUNDATION). The views, opinions and recommendations expressed herein are solely those of the authors and do not imply any endorsement by the ALPHA FOUNDATION, its directors and staff.

1.0 Executive Summary

Much of what is known about respirable coal mine dust (RCMD) in the US stems from sampling performed to demonstrate regulatory compliance. These sampling efforts yield two primary metrics: the time-weighted average mass concentration of respirable dust to which a miner was exposed, and the quartz (crystalline silica) content in that dust. Over four decades, both metrics have been on a downward trend. However, almost nothing is known about if or how *dust characteristics* (e.g., distributions of specific constituents and particles sizes) have changed. Indeed, such knowledge could help to explain the effects of different mining practices or conditions on RCMD—not to mention lending valuable insights to trends in occupational lung disease. Although recent studies, including those in our research group, have produced significant data on ‘modern’ RCMD characteristics, there is no comparable data available from earlier periods. This is simply because historical samples are scarce. For example, samples collected for regulatory compliance are no longer available for detailed characterization studies since they are typically disposed, or destructed if used for quartz analysis.

Recently, however, NIOSH located numerous ‘historical’ RCMD samples that it collected as part of a Federal research study between 2003-2005, and graciously agreed to provide them for the current research project. Notably—while these historical samples postdate the likely exposure period for many of the occupational disease cases captured by the resurgence trend beginning in the mid- to late-1990s—they predate the 2014 ‘new dust rule’ which lowered the respirable dust standard in US coal mines from 2.0 to 1.5mg/m³, as well as an increased emphasis on rock dusting following two major explosion incidents at the Sago (2006) and Upper Big Branch (2010) mines. Moreover, the NIOSH samples and a subset of samples in our own modern sample inventory (2018-2020) were collected using the same materials (i.e., PVC filters with nominal 5 µm pore size) and equipment (i.e., 10-mm nylon cyclone, air pump operated at 2 L/min), enabling direct comparisons between dust characteristics observed in both sample groups.

This project had three main objectives, all of which were completed, and primary outcomes can be summarized as follows:

Objective 1: Establish a methodology for handling the RCMD samples. Because samples were collected on PVC, direct-on-filter FTIR was possible; however, dust had to be recovered and redeposited for further analysis by SEM-EDX. The methodology is summarized in this report and will be detailed in a conference paper (Greth et al., n.d.)

Objective 2: Analyze the RCMD samples. All samples were analyzed by direct-on-filter FTIR to estimate quartz, kaolinite and calcite content, and then by SEM-EDX to determine particle mineralogy and size distributions. Results are summarized in this report and detailed data is given in the Appendices.

Objective 3: Explore temporal trends in RCMD characteristics. Results from the historical and modern samples were compared. Overall, the influence of increased rock dusting is apparent over time (i.e., from the early 2000s to late 2010s), based on observations of relatively higher

abundance of carbonate-rich particles in the modern versus the historical RCMD samples from multiple geographic regions. With respect to the central Appalachian region, the RCMD analysis indicates a slight increase in the ratio of rock strata-sourced to coal seam-sourced dust over time, which might be due to an ongoing tendency to mine somewhat more rock along with the target coal in the characteristically thin-seam mines of this region. That said, the relative increase over time in rock strata-sourced dust was mostly attributed to silicates—rather than silica. Indeed, silica abundance (based on estimates of both particle number % and mass %) was typically found to be lower in the modern RCMD samples compared to the historical samples across particular regions, including central Appalachia.

Regarding analysis of particle sizes, distributions were generally similar between the historical and modern RCMD samples for particular regions, perhaps suggesting little change in the generation and/or control of fine *dust* particles over the time period captured by this study. However, the abundance of very fine carbonaceous particles, which are often associated with diesel emissions, decreased markedly between the historical and modern samples from some regions. This might signal a reduction in use of high-emission engines over the study time period.

2.0 Problem Statement and Objective

It is now well established that there has been a resurgence of severe and rapidly progressive lung disease among central Appalachian coal miners since the late 1990s (Figure 1a; Blackley et al., 2016). However, this trend appears in stark contrast to the available respirable coal mine dust (RCMD) monitoring data since the late 1980s, which generally show declining levels of respirable dust and quartz on the basis of mass concentration (Figure 1b; Agioutanti et al., 2020 and MSHA, 2017). There has been wide speculation that changes in mining practices and technologies have led to changes in RCMD characteristics, such that exposures (even to similar or perhaps lower mass concentrations) have become more hazardous over time (e.g., see National Academies, 2018). For example, the tendency to mine increasingly thinner coal seams might have resulted in dust with a greater proportion of mineral content; and use of higher-powered drilling and cutting machinery, or even advanced dust capture systems, might have yielded dust with smaller particle sizes.

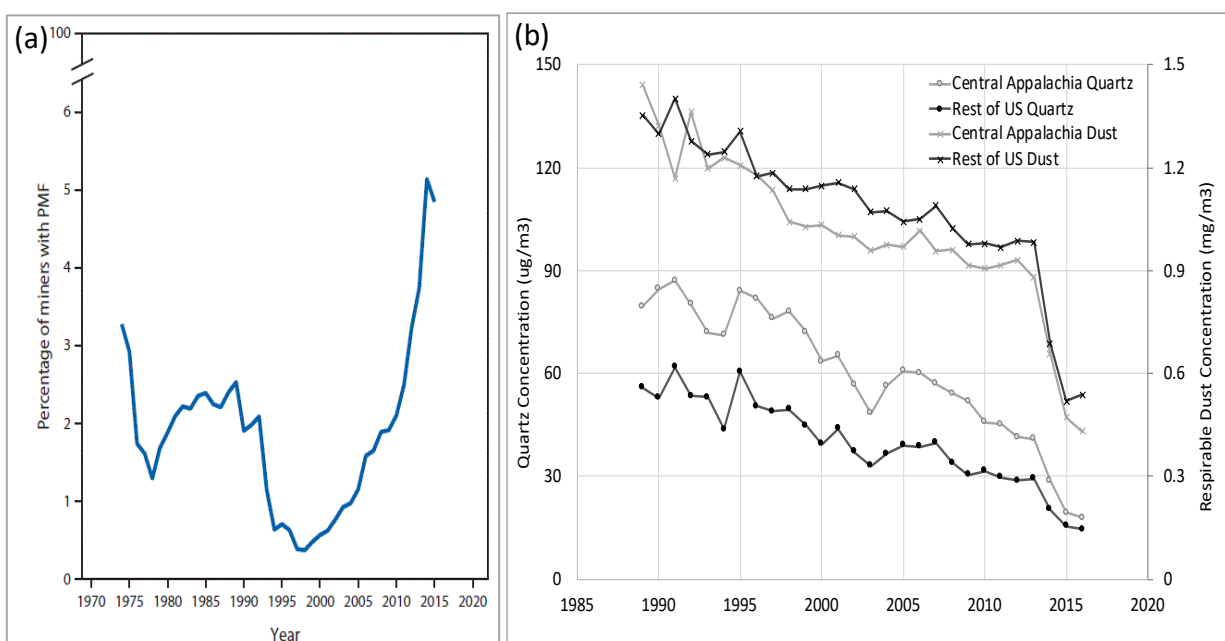


Figure 1. (a) Prevalence of progressive massive fibrosis among underground coal miners in central Appalachia based on Coal Workers' Health Surveillance Program data. (Taken from Blackley et al., 2016.) (b) Geometric mean quartz ($\mu\text{g}/\text{m}^3$) and respirable dust concentration (mg/m^3) in operator and inspector samples collected in underground coal mines in central Appalachia (MSHA districts 4, 5 and 12) and the rest of the US between 1989-2016. (Adapted from Agioutanti et al., 2020, using the original dataset from MSHA, 2017.)

Research within our own group has yielded a wealth of information regarding characteristics of respirable dust in modern mines, including on mineral constituents and particle sizes (e.g., see Sarver et al., 2021), however there is no analog for prior periods in time. Thus, while the hypothesis of changing dust characteristics is well reasoned and frequently presented, there is little hard data available for support. A recent report produced by the National Academies of Science, Engineering and Medicine (2018) specifically discussed this knowledge gap, and recommended that research be conducted to close it.

The National Academies report also included a focus on rock dusting (i.e., application of inert stone dust, usually high purity limestone or dolostone, to mitigate explosibility hazards) and the possible contribution of rock dust to the respirable fraction. While our own analysis of samples collected recently (i.e., since 2013) has shown that rock dusting can contribute to RCMD (e.g., see Sarver et al., 2021; Jaramillo et al. 2022; Pokhrel et al., 2021), it is unclear how much the situation changed following the Sago (2006) and Upper Big Branch (2010) mine explosions, which prompted greater emphasis on rock dusting efforts (Luo et al., 2017). Indeed, MSHA increased rock dusting requirements via an emergency temporary standard in late 2010, and published a final rule with the increased requirements in 2011. Moreover, the impact of the 2014 ‘new dust rule’ on RCMD characteristics has not been investigated heretofore. The rule effectively lowered the respirable dust concentration standard from 2.0 to 1.5 mg/m³ and, overall, mines have been successful in complying (see Figure 1b)—but studies have not been conducted to understand if or how RCDM characteristics have changed as dust levels have trended downward.

The specific aim of this project was to elucidate if or how RCMD characteristics, including particle size and primary constituents, have changed over time. Briefly, the research approach entailed comparison of historical and modern samples of RCMD.

- For the modern samples, our research team had samples (n=44) collected between 2018-2020. They represent 16 underground coal mines, which could be assigned to four distinct geographical regions (i.e., central Appalachia, northern Appalachia, Mid-west and West). The samples were collected in standardized locations (i.e., intake, feeder, production, bolter, and return).
- For the historical samples, NIOSH provided samples (n=59) it collected between 2003-2005, also using PVC filters and the same sampling trains. These samples represent 9 different mines, each of which could also be assigned to one of the four distinct regions. The exact sampling locations were not known for most of the NIOSH samples; however, based on the original NIOSH study design, it was deduced the samples were most likely collected in the production, bolter, or return locations.
- FTIR and SEM-EDX analysis were conducted on all the available samples. The FTIR could be performed directly on the PVC filters, however the SEM-EDX analysis required recovery of dust from the fibrous PVC filter and redeposition onto a smooth polycarbonate (PC) filter. Thus, a preliminary objective for this project was to establish a reliable sample handling and analysis method.

Accordingly, the project research plan was outlined to include three main objectives, which are shown Table 1 along with specific tasks. The sections below summarize work and outcomes for each objective.

Table 1. Project timeline showing objectives and work tasks.

2021													2022											
	J	F	M	A	M	J	J	A	S	O	N	D	J	F	M	A	M	J	J	A	S	O	N	D
Objective 1: Methodology for sample handling and analysis																								
Task 1.1: Dust recovery method																								
Task 1.2: Method validation																								
Objective 2: Dust sample analysis																								
Task 2.1: FTIR analysis																								
Task 2.2: SEM-EDX analysis																								
Objective 3: Evaluation of temporal trends																								
Task 3.1: Comparison of historical and modern dust																								

3.0 Research Approach

Sample Selection

To make direct comparisons between the historical and modern RCMD samples, and thus draw insights regarding changes in dust characteristics over time, it was critical that the sample collection, preparation and analytical procedures were the same for both groups. To this end, our early discussions with NIOSH on this project focused on determining which historical samples in their inventory could be compared to modern samples in our own inventory. Candidate samples were those that met the following criteria: dust collected on 37-mm polyvinyl chloride filter (PVC, nominal 5 μ m pore size) using standard gravimetric sampling trains (10-mm nylon cyclone, air pump operated at 2 L/min), and MSHA district and year sampled were known.

Ultimately, NIOSH was able to locate and transfer to our team 59 samples that could be used for direct comparison to our 44 available modern samples (Table 2). The historical samples were all collected between 2003-2005 (i.e., predating the 2006 Sago and 2010 Upper Big Branch mine disasters, and implementation of MSHA's 2014 'new dust rule'); and the modern samples were all collected between 2018-2020.

Table 2. Summary of historical and modern RCMD samples and analysis progress.

	Set no.	MSHA District	Year	Total
Historical	27	9	2005	4
	28	8	2005	3
	29	3	2004	13
	30	4 and 7	2005	11
	31	4 and 9	2005	11
	32	7	2005	8
	33	11	2003	9
	Total			59
Modern	10	5	2018	3
	11	5	2018	3
	12	5	2018	3
	13	5	2018	3
	14	5	2018	2
	15	4	2018	3
	16	3	2018	3
	17	3	2018	3
	18	3	2018	3
	19	8	2018	3
	20	8	2018	3
	21	12	2018	2
	22	12	2018	2
	23	9	2018	3
	24	9	2018	3
	25	12	2020	2
	Total			44

Objective 1: Methodology for sample handling and analysis

Given the scarcity of historical RCMD samples, the intrinsic value of the samples that NIOSH made available for this research was duly recognized. It was critical to establish an effective methodology for handling these samples, including recovery and redeposition of dust particles. We began by investigating both dry and wet recovery procedures. Based on early results, we determined that dry recovery was prone to loss of fine particles, which are important to questions regarding changes in dust characteristics over time; whereas the wet recovery procedure did not appear to suffer from this problem. Thus, we decided to proceed with the wet method and completed several rounds of experiments using laboratory-generated dust samples to validate the procedure. This work will be detailed in an upcoming conference paper (Greth et al., n.d.)

The final sample handling and analysis flow is shown in Figure 2 and briefly described here: First, each sample was scanned by FTIR on its original PVC filter. Next, the wet recovery procedure was performed by placing the PVC filter—or a representative section of it—into a clean glass test tube, submerging it in isopropyl alcohol (IPA), and sonicating for several minutes to release the dust particles. Then, the suspension was poured over a clean 47-mm PC filter in a vacuum filtration unit to deposit the recovered particles. (For samples with very low dust masses, the redeposition step was done by pushing the suspension through a 25-mm diameter PC filter using a syringe rather than using the vacuum filtration unit.) Once the recovered dust filter dried completely, it was prepared for SEM-EDX work. This involved cutting a 9-mm subsection and sputter coating with a thin layer of Au/PD.

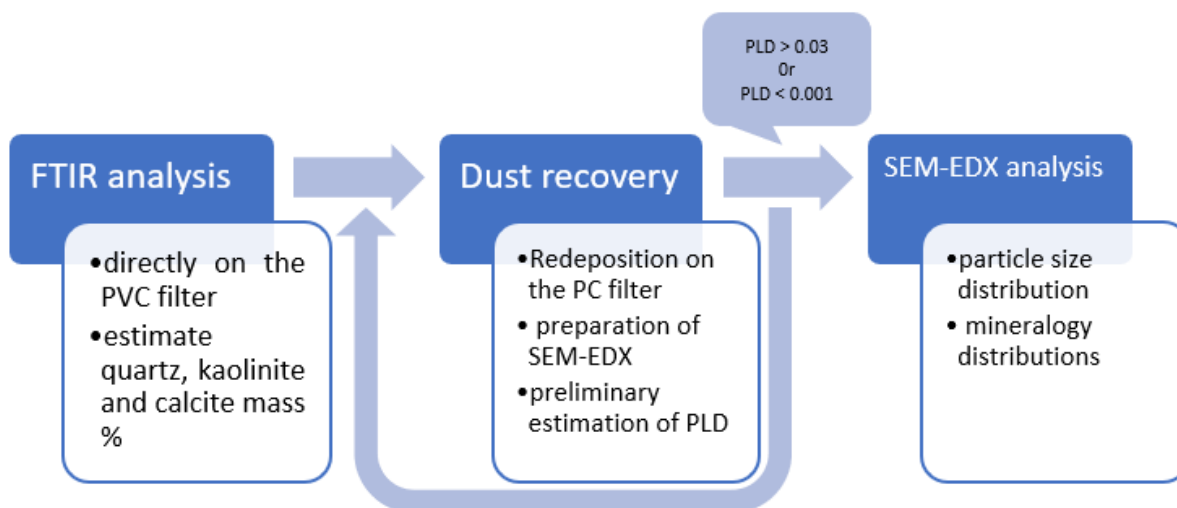


Figure 2. Schematic of dust sample handling and analysis procedure.

Under the SEM, a preliminary scan of each sample was performed to estimate the particle loading density (PLD); we have previously determined that PLD of about 0.001-0.035 particles per μm^2 is optimal to ensure enough particles can be located for characterization while also limiting interference between particles during EDX analysis (see Keles et al., 2022). For samples with PLD outside of the optimal range—which was the case for 9 modern and 13 historical samples—a new recovered dust filter was prepared, either by using a smaller section of the original PVC filter

for dust recovery or by using a smaller PC filter area for redeposition (i.e., with the syringe rather than the vacuum unit).

Objective 2: Dust sample analysis

Per Figure 2, both FTIR and SEM-EDX analysis were conducted on all the available RCMD dust samples—historical (n=59) and modern (n=44). The SEM-EDX analysis was completed using the same approach and instrumentation detailed by Sarver et al. (2021). Briefly, two separate computer-controlled routines (i.e., one for submicron particles, and one for supramicron particles) were used to size and collect elemental data on individual particles using an FEI Quanta 600 FEG environmental SEM (Hillsboro, OR, USA) equipped with a backscatter electron detector BSD and a Bruker Quantax 400 EDX spectroscope (Ewing, NJ, USA). The elemental data was used to bin each particle into a pre-defined mineralogy class (i.e., C=carbonaceous, MC=mixed-carbonaceous, ASK=kaolinite-like silicates, ASO=other aluminosilicates, SLO=other silicates, S=silica, M=heavy minerals, CB=carbonates, O=other); and the particle size and class were used to estimate the particle's mass. Then, the individual particle data was used to compute particle mineralogy and size distributions on a per sample basis.

For the FTIR analysis, we followed the approach that has been published by NIOSH (2022) for filter scanning, using an ALPHA II portable FTIR spectrometer (Bruker, Billerica, MA, USA) Bruker's OPUS software (Version 8.2.28, 32 bit). Notably, the FTIR is used to scan a 6-mm circular area in the center of the sample filter, and the quartz (or other mineral) mass computed for this area must be extrapolated to the rest of the 37-mm filter. Since dust deposition on the filter is dependent on the cassette type used to collect the sample, a cassette-specific model must be used for the extrapolation. The historical dust samples were collected in standard mine sampling cassettes (typically called "MSA" cassettes) and we computed mineral mass per filter using two different models: one derived from a seminal publication on the direct-on-filter FTIR method for RCMD samples (i.e., Miller et al., 2013), and one that is included in NIOSH's FAST software which was more recently developed to support this method. The modern dust samples were collected in generic 2-piece cassettes. While FAST does not include a model for this cassette type, we used one that could be derived from the Miller et al. (2013) work; derivation of that model has been described by Pokhrel et al., 2022.


We used the FTIR spectrum obtained for each sample to estimate quartz, kaolinite and calcite mass (μg), and then mass % using the total sample weight. For quartz, we followed method developed by NIOSH (2022). It relies on the integrated peak area corresponding to $767\text{-}816\text{ cm}^{-1}$ which must be corrected for kaolinite interference; kaolinite exhibits two peaks, with the primary at 915 cm^{-1} and the secondary at 790 cm^{-1} , respectively. As explained in detail by Pokhrel et al. (2022), since kaolinite is determined for the quartz correction, the kaolinite itself can also be reported for the sample—and we have accordingly reported kaolinite for all samples here. Moreover, we used the method described by Pokhrel et al. (2021) to estimate calcite using its characteristic spectral peak at 877 cm^{-1} .

Objective 3: Evaluation of temporal trends

Table 3 shows a summary of all samples analyzed on this project by MSHA district and geographic region, and it also shows the same summary after the samples were filtered to compare historical and modern RCMD characteristics. Filtering effectively excluded 22 historical samples from MSHA districts 7 and 11, since no modern samples were available from these districts; and 14 modern samples from intake and feeder locations were excluded, since these locations were not expected to be represented in the historical sample set.

Table 3. Summary of (top) all historical and modern RCMD samples analyzed for this project and (bottom) samples that can be reasonably compared based on similar sampling locations and mine regions. (NA=northern Appalachia, CA=central Appalachia, MW=mid-west, W=west, CKY=central Kentucky, AL=Alabama).

ALL SAMPLES									
Region	NA		CA		MW		W	CKY	AL
MSHA district	3	4	5	12	8	9	7	11	Total
Historical	13	11	-	-	3	10	13	9	59
Modern	9	3	14	6	6	6	-	-	44
FILTERED FOR COMPARISONS									
Region	NA		CA		MW		W	CKY	AL
MSHA district	3	4	5	12	8	9	7	11	Total
Historical	13	11	-	-	3	10	-	-	37
Modern	8	1	8	4	6	3	-	-	30



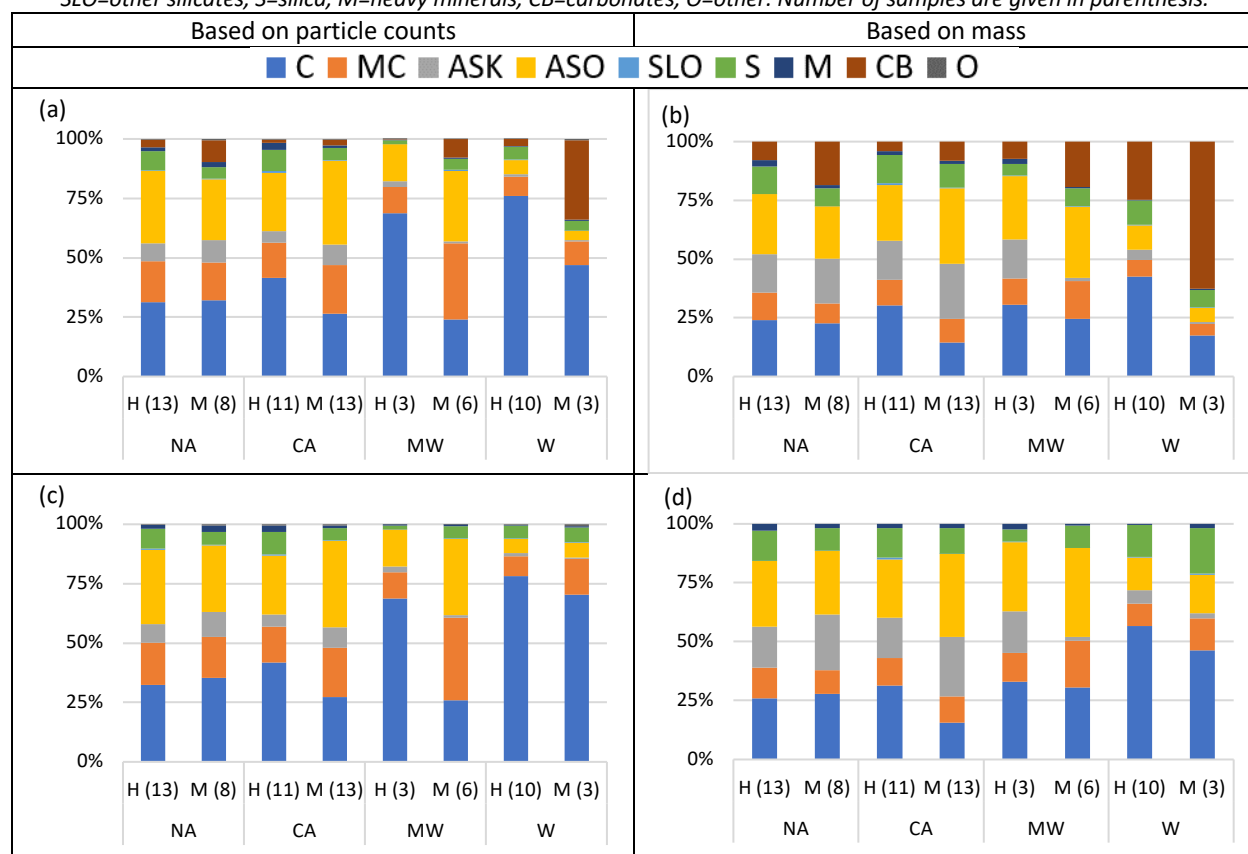
4.0 Research Findings and Accomplishments

Given the large number of RCMD samples analyzed for this project, results on a per sample basis are not included in the body of this report. However, FTIR and SEM-EDX results are tabulated in Appendix A for each sample. The sections below summarize results based on geographic region and the timeframe represented by the samples (modern or historical).

Particle mineralogy distributions (SEM-EDX)

Appendix B provides the particle mineralogy distributions derived from the SEM-EDX analysis for all samples (Tables B1-B4). Table 4 compares mineralogy distributions between the historical (n=37) and modern samples (n=30) by geographic region. Results are shown on the basis of both number % (left plots) and estimated mass % (right plots). The top plots show the distributions considering all mineralogy classes; but, in the bottom plots, the CB class is excluded (and other data normalized) to observe the RCMD constituents without the influence of rock dusting (i.e., products typically are dominated by calcium or magnesium carbonates). Overall, results indicate a higher abundance of rock dust-sourced particles in the modern samples [plots (a) and (b)], which is consistent with expectations of more rock dust application in recent years.

Table 4. Mineralogical distributions for compared samples (H=historical, M=modern) per MSHA districts based on (a) particle counts with all classes, (b) masses with all classes, (c) particle counts without carbonates (CB), (d) masses without CB. Mineralogical distribution: C=carbonaceous, MC=mixed-carbonaceous, ASK= kaolinite-like silicates, ASO=other aluminosilicates, SLO=other silicates, S=silica, M=heavy minerals, CB=carbonates, O=other. Number of samples are given in parenthesis.



When CB is excluded for the SEM-EDX results, Table 4 shows more subtle differences between the historical and modern samples—especially when results are compared on the basis of mass % [plot (d)]. Considering that we typically associate C+MC mass % with coal dust, and AS+S+SLO+M mass % with rock strata-sourced dust, it appears that modern dust samples have slightly higher abundance of rock strata-sourced dust and historical samples have slightly higher abundance of coal dust for the CA and W regions. This might be related to the tendency to mine more rock along with the coal in recent years. For samples from NA and MW, little change is observed between the proportion of dust attributed to coal and that attributed to rock strata between the historical and modern samples.

When considering silica (S), specifically, Table 4 suggests that S abundance has been reduced to some extent in CA, NA, and W mines over the time period captured by the study, which fits with trends expected from compliance monitoring data (e.g., Figure 1b). The results from MW mines would suggest the opposite—though it is important to note that relatively fewer samples were available from these regions, and of course the mines represented in the historical sample set are not necessarily the same as those represented in the modern sample set.

The clear differences in C % when the SEM-EDX data is presented on a number versus mass basis [i.e., plot (c) versus (d)] are worth discussing also. These differences are most pronounced in the samples from the MW region and are likely due to high abundance of diesel particulates. (In mines operating diesel equipment, there tend to be very large numbers of diesel particulates, but the particulates are so small that they do not contribute much to the sample mass.) Thus, a plausible interpretation of the substantial decrease in C number % in the MW region could be a trend to phase out high-emission diesel equipment.

Particle size distributions (SEM-EDX)

A comparison of cumulative particle size distributions is presented in Table 5 (for all particles; and then C, MC, ASK and ASO particles, specifically) and Table 6 (for SLO, S, M and CB particles, specifically). In Tables 5 and 6, the x-axis show the projected area diameter (PAD), which was computed based on projected area of each particle as measured by the Esprit software during the SEM-EDX computer-controlled routines. Overall cumulative particle size distributions are provided on a per sample basis in Appendix B (Tables B5-B6). (It should be noted that size distribution curves that do not appear smooth, e.g., the SLO curves, have this appearance due to very few particles in the relevant mineralogy class; so these data should be viewed with some caution.)

Table 5 (top row) indicates the overall cumulative size distributions are very similar between historical and modern samples in the NA and CA regions. For the MW and W regions, the historical samples have finer particles than modern samples. Again, this is likely due to high abundance of diesel particulates in the historical samples (i.e., fine C particles).

For particles in specific mineralogy classes, Table 5 and Table 6 show some differences between the historical and modern dust samples. Notable differences include: In the NA region, the C and MC particles tend to be slightly finer in the modern samples, but mineral dust particles show less

change (if any) between the two timeframes. This could be an indication of finer coal dust being generated (or better controlled) in NA mines more recently, without any corresponding change in the size rock-strata sourced particles. On the other hand, in the CA region, C and MC particles show little change in particle size between the historical and modern samples, whereas AS particles appear finer (and more abundant per Table 4) in the modern samples. This might be an indication of finer rock-strata sourced dust being generated more recently; that said, S particles (which are also expected to be primarily sourced from rock strata) do not follow the same trend in this region (i.e., if anything, S particles appear somewhat coarser in the modern samples).

In the MW region, most of the mineral particles appear finer in the modern dust samples—including the CB particles. While increased abundance of CB particles was expected in the modern samples from any/all regions due to increased rock dusting in recent years, we have no reason to believe that the particle size distribution of rock dust products should have changed much over time. Notably, MW is the only region where carbonate-rich rock strata is known to occur adjacent to the target coal seam in the sampled mines. Thus, the finer (and more abundant) CB particles in the modern samples are at least partially attributable to dust sourced from (carbonate-rich) roof rock. It is unknown whether the MW mines represented by the historical samples also had carbonate-rich roof rock. In this region, S appears somewhat finer in the modern than in the historical samples; this helps to explain why a relatively larger difference was observed for S number % than for S mass % between the modern and historical samples [i.e., Table 4, plot (c) versus plot (d)].

In the W region, most of the RCMD was observed to be dominated by C or CB particles (Table 4). As noted, the change in C size distribution between historical and modern samples may be at least partly due to changes in abundance of diesel particulates. While CB is much more abundant in the modern samples, the size distribution of CB is similar between the historical and modern samples. Again, this fits with expectations for CB particles primarily sourced from rock dusting.

Table 5. Averaged cumulative size distribution per sampled mine regions (NA=northern Appalachia, CA=central Appalachia, MW=mid-west, W=west) for each mineralogy classes (C=carbonaceous, MC=mixed-carbonaceous, ASK= kaolinite-like silicates, ASO=other aluminosilicates). Dashed line is for modern samples and solid line is for historical samples. (n_H =number of historical samples used in plots, n_M = number of modern samples used in plots). (PAD=projected area diameter).

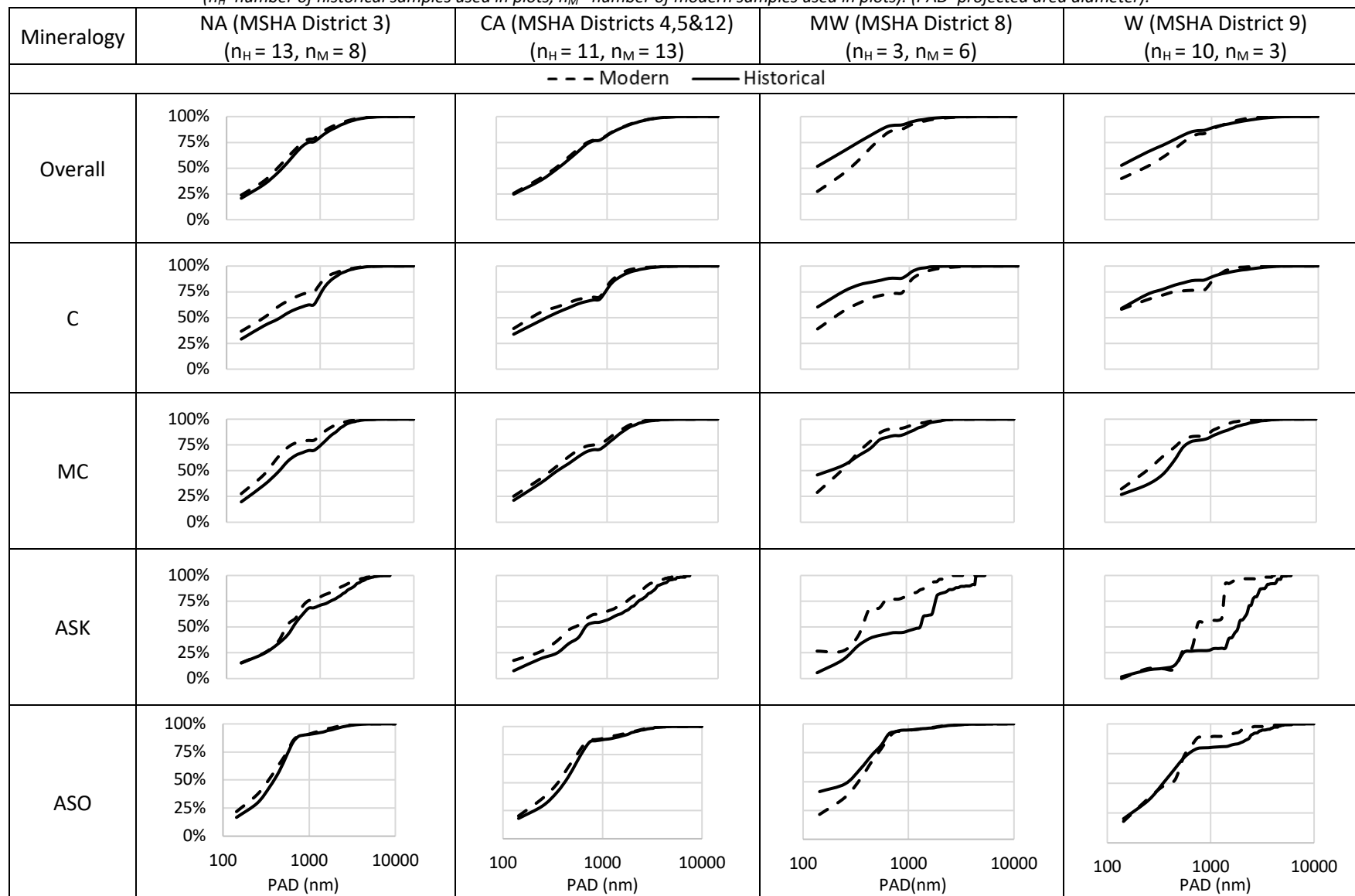
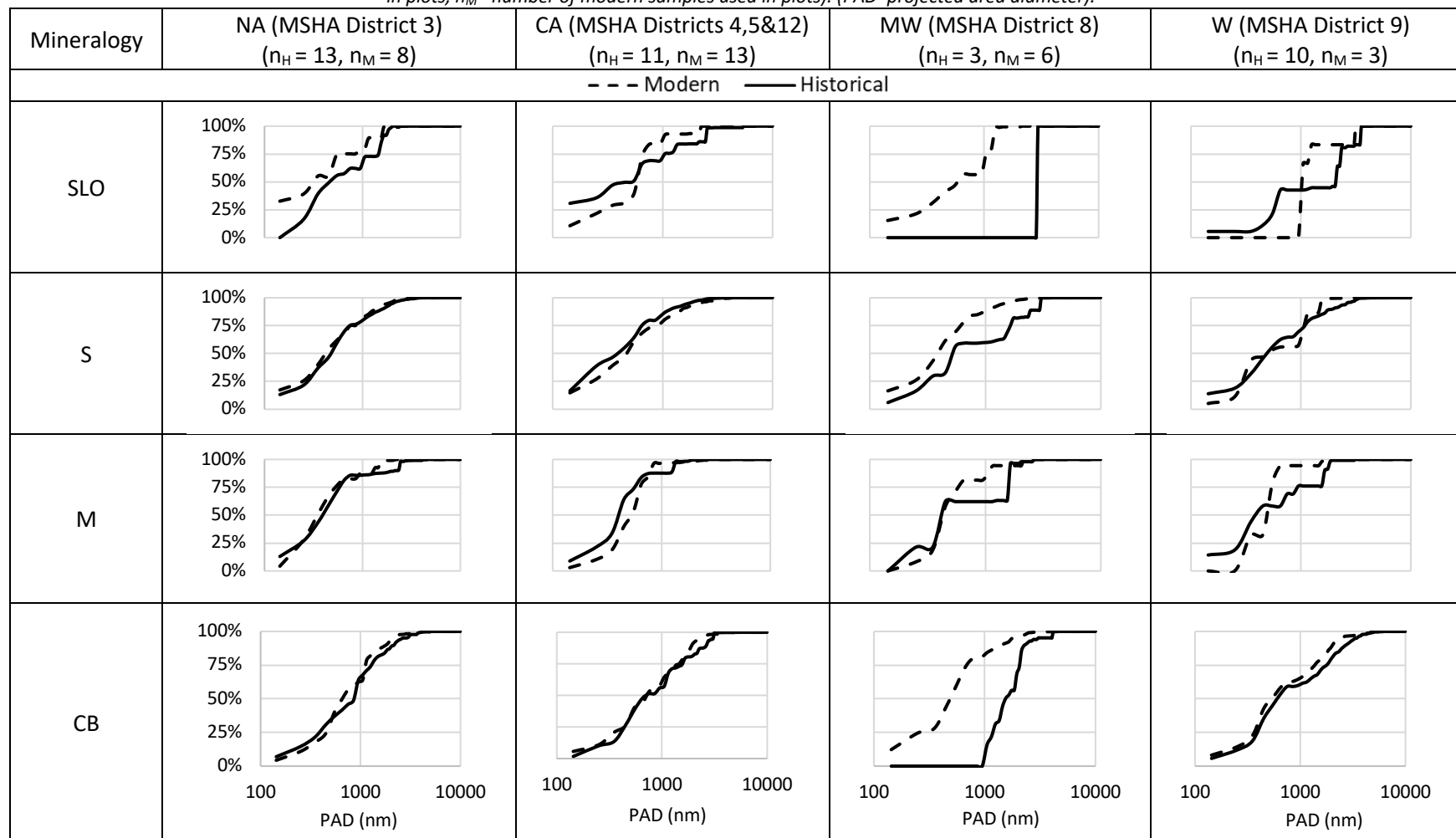


Table 6. Averaged cumulative size distribution per sampled mine regions (NA=northern Appalachia, CA=central Appalachia, MW=mid-west, W=west) for each mineralogy classes (SLO=other silicates, S=silica, M=heavy minerals, CB=carbonates). Dashed line is for modern samples and solid line is for historical samples. (n_H =number of historical samples used in plots, n_M = number of modern samples used in plots). (PAD=projected area diameter).



During the SEM-EDX analysis, images and elemental maps were periodically collected to document the appearance of particles in the different samples. Example images are included Appendix C. The images indicate that the dust recovery and redeposition process worked similarly for the modern and historical dust samples (e.g., no noticeable contamination from the original PVC filter, good dispersion of particles on the new PC filter). Further, no remarkable differences were observed with respect to particle shapes with respect to the sample being from the modern versus historical group.

Estimates of quartz, kaolinite and calcite content (FTIR)

FTIR data was collected on all samples included in this project and used to estimate quartz, kaolinite and calcite content (%) (see Appendix A). It should be noted that we cautiously approached interpretation of the FTIR results due to several limitations, including the relatively low total dust mass for many samples, and the uncertainty regarding which extrapolation model should be used to translate the FTIR spectrum observed on the center of the historical samples (collected on MSA cassettes) to the entire filter area.

Appendix D presents further explanation of these limitations and our efforts to assess them by comparing the FTIR-derived quartz, kaolinite, and calcite and SEM-EDX-derived silica, kaolinite-like silicates, and carbonates. In summary, we found that low sample mass, per se, likely had a more pronounced effect on the FTIR data obtained for the modern dust samples. Additionally, we found that using the extrapolation model based on work by Miller et al. (2013) for the historical samples yielded more similar FTIR-to-SEM-EDX correlations between the historical and modern samples.

Overall, we concluded that the FTIR data generally support the trends observed in the SEM-EDX data—meaning that relatively high abundance of silica, kaolinite-like silicates, or carbonates indicated by SEM-EDX measurements are generally echoed by relatively high silica, kaolinite, or calcite content measured by the FTIR (Figure 3). Table 7 shows the FTIR and SEM-EDX results for comparable mineral constituents, with results summarized for the historical and modern samples by geographic region.



Figure 3. FTIR-derived mass % of (a) calcite, (b) kaolinite or (c) quartz versus SEM-EDX derived mass % of (a) carbonates, (b) kaolinite-like silicates, or (c) silica. Results for modern and historical dust samples are shown separately. The open points show all samples; the solid points show samples with total mass > 100 µg.

Table 7. Summary of FTIR and SEM-EDX results (mass %) for the historical and modern samples by geographic region. For FTIR: Q=quartz, K=kaolinite, Cl=calcite. For SEM-EDX: S=silica, ASK=kaolinite-like silicates, CB=carbonates.

Region	MSHA District		FTIR									SEM-EDX (mass)					
			Historical (FAST)			Historical (Miller et al., 2003)*			Modern (Pokhrel, 2021; 2022)			Historical			Modern		
			Q	K	Cl	Q	K	Cl	Q	K	Cl	S	ASK	CB	S	ASK	CB
NA	3	n	7	12	11	7	12	11	0	7	7	13	13	13	8	8	8
		Mean (%)	9.5	19.0	11.9	6.4	12.9	8.0	-	20.2	19.3	11.6	16.2	7.9	7.6	19.3	18.4
		SD (%)	4.7	6.0	19.1	3.2	4.1	12.9	-	9.9	25.6	9.0	6.6	10.3	7.8	15.9	25.5
CA	4, 5, 12	n	7	10	7	7	10	7	6	13	6	11	11	11	13	13	13
		Mean (%)	13.7	14.7	9.2	9.3	10.0	6.2	4.4	17.5	11.9	12.1	16.6	4.0	10.1	23.4	8.0
		SD (%)	2.8	9.4	10.1	1.9	6.4	6.9	0.5	0.4	3.4	7.4	8.6	5.6	5.2	6.5	4.4
MW	8	n	0	2	3	0	2	3	1	6	6	3	3	3	6	6	6
		Mean (%)	-	11.9	2.5	-	8.0	1.7	0.5	8.6	13.2	4.8	16.4	7.3	7.5	1.4	19.3
		SD (%)	-	15.5	3.0	-	10.5	2.0	-	2.4	7.8	1.4	10.1	6.9	4.2	0.7	10.2
W	9	n	5	7	10	5	7	10	0	3	3	10	10	10	3	3	3
		Mean (%)	8.1	10.7	24.2	5.5	7.2	16.4	-	9.0	51.0	10.2	4.3	24.7	7.2	0.8	62.6
		SD (%)	5.3	5.4	22.7	3.6	3.7	15.3	-	9.5	36.2	10.4	4.1	13.8	12.2	1.2	32.9
CKY	7	n	8	10	5	8	10	5	0	0	0	13	13	13	0	0	0
		Mean (%)	22.1	20.9	4.2	14.9	14.2	2.8	-	-	-	18.6	17.5	1.3	-	-	-
		SD (%)	25.8	7.7	4.1	17.4	5.2	2.7	-	-	-	18.0	10.8	1.9	-	-	-
AL	11	n	7	9	9	7	9	9	0	0	0	9	9	9	0	0	0
		Mean (%)	5.0	12.0	17.6	3.4	8.2	11.9	-	-	-	13.3	12.4	22.3	-	-	-
		SD (%)	1.6	6.3	6.2	1.1	4.3	4.2	-	-	-	5.1	8.7	11.5	-	-	-

*Analysis of FTIR to SEM-EDX data correlations suggests that the FTIR results derived from the Miller et al. model for the historical samples should be used for comparison the FTIR results for the modern samples.

5.0 Publication Record and Dissemination Efforts

The following publications and presentations are associated with the work completed on this project:

1. Greth, A., Afrouz, S., Keles, C., Animah, F., Sarver, E., (n.d.) Recovery of respirable dust from fibrous filters for particle analysis by scanning electron microscopy. *In review for inclusion in the 19th North American Mine Ventilation Symposium.*
2. Keles, C., Afrouz, S., Sarver, E. Changes in RCMD from early 2000's to late 2010's, accepted for 2023 SME Meeting and Expo, Denver, CO.
3. Afrouz, S., Keles, C., Sarver, E. A Study of Temporal Trends in Respirable Coal Mine Dust Characteristics, presented at the 2022 Annual SME Meeting and Expo, Salt Lake City, UT.

We are also planning at least two journal publications to present project findings:

4. Keles, C., Afrouz, S., Sarver, E., Respirable dust characteristics in US coal mines before and after the 2014 'New dust rule', target: Journal of Occupational and Environmental Hygiene.
5. Greth, A., Afrouz, S., Keles, C., Sarver, E., Respirable coal mine dust characteristics by SEM using direct-on-filter versus recovered dust analysis, target: Mining, Metallurgy and Exploration.*

*Notably, because the modern samples (originally on PVC filters) used for this project were actually collected in tandem with samples on PC filters, this follow-up effort is planned to compare the SEM-EDX results from analysis of recovered dust samples (on this project) to those yielded by the direct-on-PC analysis (conducted on prior projects).

6.0 Conclusions and Impact Assessment

The historical samples available for this project are not old enough to evaluate RCMD characteristics from the time period(s) of most interest for understanding the occupational disease recurrence among US coal miners that began in the mid- to late-1990s. That said, valuable insights might still be drawn from an understanding of dust characteristics in 2003-2005. Further, a comparison of the historical and modern samples here enable important understanding of dust before and after two major efforts by MSHA: (1) increased rock dusting requirements that were effectively implemented in 2010, and (2) a lowered respirable dust standard that was implemented by a 'new dust rule' in 2014.

Overall, results from this project do suggest that an increased emphasis on rock dusting has resulted in a somewhat higher proportion of rock dust-sourced particles in RCMD. Of course, the increased emphasis on rock dusting has also coincided with an increased emphasis on reducing total RCMD concentration—mostly via improved ventilation and dust controls, designed to reduce the dust generated from cutting/drilling into the geologic strata. When the results are normalized to exclude particles typically associated with rock dusting (i.e., carbonates), it appears that ratios of particles likely sourced from coal (i.e., carbonaceous) and rock strata (i.e., silicates, silica) have not changed as much. This suggests that efforts to reduce RCMD concentration have not been differentially effective with respect to rock-strata versus coal-sourced dust. Nevertheless, prior work by our group (on modern samples) has indicated that cutting rock generates an inordinate amount of respirable dust relative to cutting coal (e.g., see Sarver et al., 2021; Jaramillo et al., 2022); and the results presented here indicate this was also true in the early 2000's. In the central Appalachian region, specifically, a relative increase in the rock-strata to coal-sourced dust ratio was observed between the historical and modern RCMD samples, and this might be related to mining even more rock along with the target coal over time.

Size distributions measured here did not reveal substantial changes between the historical and modern samples for the dominant particle types in most cases. One exception was the reduction in very fine carbonaceous particles over time in the mid-western region. Since these particles are frequently associated with diesel emissions, this observation might signal a phasing out of high-emission engines. In the mid-western region, an apparent change in both the relative abundance (more over time) and size (finer over time) of carbonate particles was also observed. Given knowledge of limestone roof strata in the mid-western mines where the modern dust samples were collected, an abundance of fine carbonate particles was expected in these samples (e.g., due to drilling/cutting in the roof strata). However, what we cannot assess with certainty is whether the difference between the historical and modern samples truly represents a change over time for the region—because the apparent change could easily have more to do with the specific mines sampled during each time frame than any particular changes in roof rock extraction that might have occurred region-wide.

Indeed, a primary limitation of the current work is that, while the historical and modern sampling procedures and analyses were the same, the mines sampled during each time frame were not.

(At least, we did not have any identifying information for the mines where the historical samples were collected, so we cannot claim any direct comparisons per mine.) Thus, we chose to group samples by MSHA district, and then geographic region based on the assumption that RCDM characteristics should vary by region; this assumption is supported by our prior work (e.g., see Sarver et al., 2021) but must be acknowledged, nonetheless. Likewise, since we only had general information regarding the sampling locations for the historical samples, we cannot make direct comparisons between specific locations over time. Knowing that the historical samples were collected in the vicinity of designated occupations, we chose to compare them only with our modern samples that were collected nearby to production, bolting or in the return airway; we assumed that our modern intake and feeder location samples are probably not comparable to the historical samples.

Despite significant interest in the topic, evaluating temporal trends in RCMD characteristics is inherently challenging. This is because historical data is scarce, and historical dust samples are not widely available. This project represents an important step forward though. With cooperation from NIOSH to provide what historical samples could be found from their prior work, we were able to analyze a substantial number of samples dating to the early 2000's—and we were able to directly compare results with more modern samples collected just a few years ago, because all samples had been collected using the same materials and procedures. The method developed herein for respirable dust sample handling and analysis could be applied to other samples (if any can be located), and itself represents a key contribution to the field. Further, our effort to compare dust constituent results derived from the direct-on-filter FTIR method and the SEM-EDX method may provide useful data for those wanting to apply either method.

Overall, the data gathered on this project might be valuable to inform work in areas such as dust toxicity, epidemiology, and dust control and monitoring technologies.

7.0 Recommendations for Future Work

Related to RCMD characterization, two main recommendations for future work include:

- *Collection and analysis of additional modern RCMD samples to enable complete comparison to historical sample set represented here.* While we were able to obtain and analyze historical RCMD samples from central Kentucky (former MSHA district 7) and Alabama (former district 11), we did not have any modern samples from those regions. Especially since the historical samples indicated relatively high silica content, an effort should be made to evaluate modern RCMD from those regions.
- *Exploration of possibilities to obtain additional historical dust samples.* The current project achieved important first steps for historical RCMD analysis, including establishing sample selection protocols and analytical methods. However, to move this work forward, it is critical to identify more historical samples—or ways in which historical RCMD could be recreated. Ideally, the latter could be achieved in head-to-head tests of modern equipment versus older model equipment (or at least modern equipment retrofitted or operated to mimic dust generation/control from older equipment). This might be possible in a real or test mine with both coal and representative rock strata available for cutting. Certainly, other experimental designs may also be possible, especially in collaboration with key partners such as equipment manufacturers and experienced miners.

8.0 References

1. Agioutanti, E., Keles, C., & Sarver, E. (2020). A thermogravimetric analysis application to determine coal, carbonate, and non-carbonate minerals mass fractions in respirable mine dust. *Journal of Occupational and Environmental Hygiene*, 17(2-3), 47-58.
2. Blackley, D.J., Crum, J.B., Halldin, C.N., et al. (2016) Resurgence of progressive massive fibrosis in coal miners - Eastern Kentucky. *MMWR*, 65(49), 1385–1389.
3. Jaramillo, L., Agioutanti, E., Keles, C. & Sarver, E. (2022). Thermogravimetric Analysis of Respirable Coal Mine Dust for Source Apportionment, *Journal of Environmental and Occupational Health*, 19(9), 568-579.
4. Keles, C., Pokhrel, N., & Sarver, E. (2022) A study of respirable silica in underground coal mines: Sources. *Minerals*, 12: 1115.
5. Luo, Y., Wang, D. & Cheng, J. (2017) Effects of rock dusting in preventing and reducing intensity of coal mine explosions. *Int J Coal Sci Technol*, 4, 102–109.
6. Miller et al. (2013) Deposition Uniformity of Coal Dust on Filters and Its Effect on the Accuracy of FTIR Analyses for Silica. *Aerosol Sci. Technol.* 47(7): 724-733.
7. Mine Safety and Health Administration (MSHA) (2017) Complete Quartz Data (1986-2016), Retrieved from: <https://www.msha.gov/news-media/special-initiatives/2016/09/28/respirable-dust-rule-historic-step-forward-effort-end>
8. National Academies of Sciences, Engineering, and Medicine (NASEM) (2018) Monitoring and Sampling Approaches to Assess Underground Coal Mine Dust Exposures. Washington, DC: The National Academies Press.
9. National Institute of Occupational Safety and Health (NIOSH) (2022) Direct-on-filter analysis for respirable crystalline silica using a portable FTIR instrument. By Chubb LG, Cauda EG. Pittsburgh PA: U.S. Department of Health and Human Services, Centers for Disease Control and Prevention, National Institute for Occupational Safety and Health, DHHS (NIOSH) Publication No. 2022–108, IC 9533.
10. Pokhrel, N., Keles, C., Jaramillo, L., Agioutanti, E., & Sarver, E. (2021) Direct-on-Filter FTIR Spectroscopy to Estimate Calcite as A Proxy for Limestone ‘Rock Dust’ in Respirable Coal Mine Dust Samples. *Minerals*. 11(9):922.
11. Pokhrel, N., Agioutanti, E., Keles, C., Afrouz, S., & Sarver, E. (2022). Comparison of respirable coal mine dust constituents estimated using FTIR, TGA, and SEM-EDX. *Mining Metallurgy and Exploration*, 39, 291-300.
12. Sarver, E., Keleş, C., & Afrouz, S. (2021) Particle size and mineralogy distributions in respirable dust samples from 25 US underground coal mines. *International Journal of Coal Geology*, 247: 103851.

9.0 Additional Acknowledgements

We thank the Alpha Foundation for the Improvement of Mine Safety and Health for funding this work. We gratefully acknowledge the CDC/NIOSH Mining Research Division for provision of the historical dust samples investigated on this project. In particular, we thank George Luxbacher, Jay Colinet and Milan Yekich for their support and assistance in putting together the sample inventory and associated documentation. We also appreciate the many mine partners who provided mine access and logistical support for collection of the modern dust samples investigated here.

10.0 Appendices

Appendix A: FTIR and SEM-EDX results per sample

Table A1. FTIR data summary per sample. For modern samples, FTIR mass% was calculated based on Pokhrel et al. (2021; 2022), for historical samples, it was calculated with equations in FAST (on the left column) and Miller et al. (2013) (on the right column). Mine region: NA=northern Appalachia, CA=central Appalachia, CKY=central Kentucky, MW=mid-west, W=west, AL=Alabama; mineralogical distribution: Q=quartz, K=kaolinite, Cl=calcite. Sampling location: B=bolter, P=production, R=return, I=intake, F=feeder, LW=longwall mining, CM=continuous miner. Time: M=Modern, H=Historical.

No	Mine /Set	MSHA District	Region	Sampling Location	State	Year	Time	Dust Weight (mg)	FTIR mass%		
									Q	K	Cl
1	11	5	CA	P	VA	2018	M	1.153	6.2	10.5	
2	11	5	CA	B	VA	2018	M	0.106		21.4	4.8
3	11	5	CA	F	VA	2018	M	0.164		12.5	3.0
4	15	4	CA	B	WV	2018	M	0.145		17.2	12.6
5	15	4	CA	I	WV	2018	M	0.470		2.1	1.1
6	15	4	CA	F	WV	2018	M	0.028		49.4	27.2
7	12	5	CA	I	VA	2018	M	0.054		31.0	14.1
8	12	5	CA	P	VA	2018	M	1.077	4.0	11.3	
9	12	5	CA	B	VA	2018	M	0.103		18.4	17.3
10	14	5	CA	F	VA	2018	M	0.187		16.7	
11	14	5	CA	B	VA	2018	M	0.039		37.5	7.2
12	18	3	NA	R	WV	2018	M	0.231		20.1	1.6
13	18	3	NA	P	WV	2018	M	0.340		19.2	
14	18	3	NA	B	WV	2018	M	0.096		29.2	4.6
15	17	3	NA	P	WV	2018	M	0.277		22.5	0.4
16	17	3	NA	B	WV	2018	M	0.043		34.5	52.7
17	17	3	NA	R	WV	2018	M	0.489		5.2	59.8
18	16	3	NA	P	WV	2018	M	0.221		11.7	4.9
19	16	3	NA	B	WV	2018	M	0.089		18.5	10.9
20	16	3	NA	F	WV	2018	M	0.073		31.2	9.4
21	19	8	MW	P	IL	2018	M	0.277		7.3	17.1
22	19	8	MW	R	IL	2018	M	0.299		6.5	19.1
23	19	8	MW	B	IL	2018	M	0.181		13.3	5.6
24	20	8	MW	P	IL	2018	M	0.758	0.5	7.9	6.0
25	20	8	MW	R	IL	2018	M	0.577		8.5	7.4

26	20	8	MW	B	IL	2018	M	0.530					8.3	23.8
27	13	5	CA	F	VA	2018	M	0.189					7.4	13.5
28	13	5	CA	I	VA	2018	M	0.035					37.8	67.0
29	13	5	CA	R	VA	2018	M	1.297	1.8				2.3	3.5
30	10	5	CA	P	KY	2018	M	1.494					18.7	
31	10	5	CA	F	KY	2018	M	0.183					16.0	
32	10	5	CA	B	KY	2018	M	0.181					23.1	
33	22	12	CA	F	WV	2018	M	0.018					68.5	
34	22	12	CA	I	WV	2018	M	0.003					445.2	
35	21	12	CA	B	WV	2018	M	0.085					18.0	14.8
36	21	12	CA	R	WV	2018	M	0.557	4.4				11.2	
37	23	9	W	I	CO	2018	M	0.176					7.2	29.3
38	23	9	W	R	CO	2018	M	0.888					3.6	55.6
39	23	9	W	P	CO	2018	M	0.349					3.4	84.7
40	24	9	W	R	CO	2018	M	0.068					20.0	12.6
41	24	9	W	F	CO	2018	M	5.361	3.5				2.8	74.7
42	24	9	W	I	CO	2018	M	0.052					18.5	18.3
43	25	12	CA	B	WV	2020	M	0.392	7.6				18.6	
44	25	12	CA	P	WV	2020	M	0.193	2.2				21.9	
45	27	9	W	A - MMU A	UT	2005	H	0.805	2.8	1.9	4.7	3.2	5.7	3.8
46	27	9	W	A - MMU B	UT	2005	H	0.737	9.3	6.3	4.1	2.8	32.7	22.1
47	27	9	W	C	UT	2005	H	0.210	4.7	3.2			5.6	3.8
48	27	9	W	B	UT	2005	H	0.143					12.2	8.3
49	28	8	MW	B - MMU A	IL	2005	H	5.321			0.9	0.6	0.2	0.1
50	28	8	MW	A	IL	2005	H	0.409			22.8	15.5	1.3	0.9
51	28	8	MW	B - MMU B	IL	2005	H	0.197					5.9	4.0
52	29	3	NA	A	WV	2004	H	1.169	6.6	4.4	21.0	14.2	0.6	0.4
53	29	3	NA	F	WV	2004	H	1.118	11.0	7.5	13.9	9.4	0.7	0.5
54	29	3	NA	B - MMU D	WV	2004	H	0.987	7.6	5.1	17.0	11.5	56.0	37.8
55	29	3	NA	B - MMU C	WV	2004	H	0.607	2.3	1.5	16.1	10.9	43.3	29.3
56	29	3	NA	D	WV	2004	H	0.414	17.2	11.6	17.6	11.9	1.2	0.8
57	29	3	NA	B - MMU A	WV	2004	H	0.416			21.0	14.2	4.8	3.3

58	29	3	NA	G	WV	2004	H	0.388			19.1	13.0	4.1	2.7
59	29	3	NA	C	WV	2004	H	0.281	9.5	6.4	15.6	10.6	5.8	3.9
60	29	3	NA	E	WV	2004	H	0.257			14.5	9.8	1.1	0.8
61	29	3	NA	B - MMU B	WV	2004	H	0.270			13.2	9.0	9.8	6.6
62	29	3	NA	A	WV	2004	H	0.211			23.4	15.9	3.6	2.4
63	29	3	NA	B	WV	2004	H	0.170	12.2	8.3	35.2	23.9		
64	30	4	CA	C	WV	2005	H	1.889	14.6	9.9	5.9	4.0		
65	30	7	CKY	D	KY	2005	H	1.124	3.8	2.6	16.4	11.1		
66	30	7	CKY	E	KY	2005	H	0.959	39.5	26.7	17.6	11.9	2.9	1.9
67	30	4	CA	A	WV	2005	H	0.953			1.6	1.1	11.5	7.8
68	30	4	CA	F	WV	2005	H	0.473			3.8	2.6	1.1	0.8
69	30	4	CA	B	WV	2005	H	0.162	10.9	7.4	9.0	6.1	3.1	2.1
70	30	4	CA	D	WV	2005	H	0.139	13.9	9.4	15.6	10.6	5.1	3.4
71	30	4	CA	E	WV	2005	H	0.038						
72	31	4	CA	A	WV	2005	H	3.280	15.9	10.7	21.8	14.8		
73	31	4	CA	D	WV	2005	H	1.387	18.0	12.2	28.3	19.2		
74	31	4	CA	E	WV	2005	H	1.074	10.0	6.8	25.4	17.2	2.1	1.4
75	31	4	CA	B	WV	2005	H	0.749	12.9	8.7	14.0	9.5	11.5	7.8
76	31	9	W	D	CO	2004	H	0.671	7.2	4.9	15.0	10.2	9.5	6.4
77	31	9	W	B	CO	2004	H	0.560	16.6	11.2	17.8	12.0	16.4	11.1
78	31	9	W	C	CO	2004	H	0.427			8.1	5.5	79.3	53.6
79	31	9	W	A - LW	CO	2004	H	0.171			15.3	10.4	15.3	10.3
80	31	9	W	A - CM	CO	2004	H	0.153			9.8	6.7	22.9	15.4
81	31	9	W	E	CO	2004	H	0.090					42.7	28.9
82	31	4	CA	C	WV	2005	H	0.046			21.8	14.8	30.1	20.4
83	32	7	CKY	F	KY	2005	H	1.393	5.1	3.5	15.6	10.6		
84	32	7	CKY	H	KY	2005	H	1.174	21.7	14.7	20.5	13.9		
85	32	7	CKY	C	KY	2005	H	1.098	10.7	7.2	22.2	15.0	1.1	0.8
86	32	7	CKY	D	KY	2005	H	1.034	78.8	53.2	10.8	7.3	4.0	2.7
87	32	7	CKY	E	KY	2005	H	1.031	4.6	3.1	16.9	11.4		
88	32	7	CKY	B	KY	2005	H	0.890	12.4	8.4	21.3	14.4		
89	32	7	CKY	A	KY	2005	H	0.272			31.0	21.0	1.7	1.2

90	32	7	CKY	G	KY	2005	H	0.028			36.8	25.0	11.2	7.6
91	33	11	AL	P	AL	2003	H	0.496	6.5	4.4	13.2	8.9	18.0	12.2
92	33	11	AL	B	AL	2003	H	0.463	5.6	3.8	15.8	10.7	26.0	17.6
93	33	11	AL	B	AL	2003	H	0.390	5.8	3.9	20.0	13.6	6.0	4.1
94	33	11	AL	B	AL	2003	H	0.299	6.6	4.5	13.3	9.0	25.1	16.9
95	33	11	AL	P	AL	2003	H	0.095			21.8	14.8	19.1	12.9
96	33	11	AL	P	AL		H	0.455			6.6	4.4	15.1	10.2
97	33	11	AL	B	AL		H	0.487	2.5	1.7	6.7	4.5	20.9	14.1
98	33	11	AL	P	AL		H	0.608	5.0	3.4	4.5	3.0	13.3	9.0
99	33	11	AL	B	AL		H	0.553	3.1	2.1	6.6	4.5	15.0	10.1
100	30	7	CKY			2005	H							
101	30	7	CKY			2005	H							
102	29	3	NA			2004	H							
103	30	7	CKY			2005	H							

Table A2. SEM-EDX data summary per sample based on particle counts and mass. Mine region: NA=northern Appalachia, CA=central Appalachia, CKY=central Kentucky, MW=mid-west, W=west, AL=Alabama; mineralogical distribution: C=carbonaceous, MC=mixed-carbonaceous, ASK=kaolinite-like silicates, ASO=other aluminosilicates, SLO=other silicates, S=silica, M=heavy minerals, CB=carbonates, O=other. Time: M=Modern, H=Historical.

No	MSHA District	Mine Region	Time	SEM-EDX particle counts %										SEM-EDX mass %							
				C	MC	ASK	ASO	SLO	S	M	CB	O	C	MC	ASK	ASO	SLO	S	M	CB	
1	5	CA	M	19.7	20.1	10.3	41.0	1.3	5.8	1.2	0.3	0.2	7.3	9.6	22.3	52.0	0.1	7.9	0.3	0.4	
2	5	CA	M	21.0	17.0	6.9	43.0	0.6	6.2	1.5	2.8	0.9	5.4	9.6	18.0	49.9	0.1	9.2	3.3	4.6	
3	5	CA	M	39.3	16.4	2.0	21.3	0.3	3.6	12.0	3.8	1.2	34.7	17.0	9.7	14.3	0.2	3.3	17.9	2.9	
4	4	CA	M	24.6	21.1	7.3	36.3	0.2	6.1	0.7	3.2	0.4	15.7	9.0	18.6	27.1	0.0	16.1	0.4	13.1	
5	4	CA	M	61.3	6.5	0.0	7.6	0.0	0.3	0.0	24.2	0.0	6.8	2.9	0.5	4.4	0.2	0.7	0.0	84.6	
6	4	CA	M	59.3	10.7	7.8	8.7	0.1	6.2	0.0	7.2	0.1	22.6	3.6	33.9	12.5	0.1	15.5	0.0	11.8	
7	5	CA	M	82.6	6.3	1.1	7.0	0.0	0.1	0.0	2.5	0.3	48.4	11.8	7.8	8.6	0.3	5.2	0.0	17.8	
8	5	CA	M	17.1	17.4	7.9	49.7	0.0	4.9	2.2	0.6	0.3	14.9	12.2	26.5	35.3	0.0	9.7	1.1	0.2	
9	5	CA	M	51.2	13.4	3.2	21.8	0.0	2.1	1.8	6.0	0.5	22.4	7.1	9.6	21.5	0.0	5.3	2.2	31.8	
10	5	CA	M	9.9	20.4	5.6	51.5	0.3	5.5	5.3	1.3	0.3	7.9	10.0	19.2	49.2	0.2	8.0	4.1	1.5	
11	5	CA	M	22.0	22.4	4.7	37.7	0.8	6.8	2.6	2.7	0.2	4.8	8.9	13.9	52.7	0.1	9.2	5.1	5.3	
12	3	NA	M	18.0	16.6	13.2	47.3	0.0	4.0	0.0	0.6	0.3	8.1	7.0	26.7	49.0	0.0	7.7	0.0	1.6	
13	3	NA	M	18.0	15.2	14.9	47.0	0.0	3.9	0.3	0.0	0.6	14.3	4.6	31.2	46.2	0.0	3.2	0.3	0.1	
14	3	NA	M	28.8	22.8	9.1	33.3	0.3	3.6	0.1	1.6	0.5	14.6	9.1	29.0	32.3	0.0	10.6	0.7	3.8	
15	3	NA	M	16.4	14.0	21.7	40.8	0.3	2.9	2.4	0.9	0.6	10.6	7.7	45.0	30.5	0.0	3.3	2.2	0.8	
16	3	NA	M	28.3	10.6	3.6	3.1	0.8	15.9	1.6	36.1	0.0	19.1	3.8	6.1	1.5	0.5	25.5	1.2	42.2	
17	3	NA	M	43.7	13.4	3.6	5.6	0.3	3.0	0.2	29.1	1.0	21.6	3.9	0.4	1.3	0.0	1.5	0.0	71.3	
18	3	NA	M	48.6	16.8	4.9	15.9	0.1	3.0	8.0	1.7	1.1	50.8	14.8	4.0	8.5	0.2	4.4	3.4	13.9	
19	3	NA	M	55.8	16.4	4.4	12.5	0.0	2.3	5.8	2.1	0.7	42.4	15.3	12.2	7.6	0.0	4.7	4.4	13.3	
20	3	NA	M	48.2	14.8	7.1	19.6	0.0	1.2	4.7	3.8	0.6	40.9	12.4	20.6	9.9	0.0	3.0	2.4	10.7	
21	8	MW	M	36.5	30.7	0.8	15.9	0.0	3.3	0.1	12.6	0.0	23.9	16.5	0.8	25.4	0.0	2.8	0.8	29.7	
22	8	MW	M	25.2	25.0	0.3	26.7	1.0	4.8	2.0	14.6	0.3	24.7	12.0	0.6	23.5	0.3	7.8	1.1	29.9	
23	8	MW	M	19.6	34.2	1.7	31.6	0.0	10.9	0.9	1.0	0.0	23.4	18.2	1.3	39.7	0.1	10.5	0.9	5.9	
24	8	MW	M	14.6	31.7	0.4	45.0	0.6	3.1	0.6	4.0	0.0	27.8	16.4	1.0	36.3	0.4	5.5	0.4	12.1	
25	8	MW	M	27.3	32.9	1.7	33.3	0.6	1.8	0.3	2.1	0.0	28.0	17.7	2.7	33.4	0.2	4.5	0.2	13.4	
26	8	MW	M	20.5	37.8	0.5	25.3	0.0	3.5	0.3	11.9	0.1	19.6	15.6	1.7	23.8	0.1	14.1	0.4	24.8	
27	5	CA	M	84.7	3.9	0.5	3.9	0.0	1.1	0.9	4.9	0.0	51.9	6.0	8.7	6.4	0.0	8.1	0.3	18.6	
28	5	CA	M	40.2	11.5	0.7	5.1	1.0	3.0	1.9	36.5	0.1	12.9	4.3	1.3	7.7	0.0	3.3	0.1	70.3	

29	5	CA	M	49.6	9.9	8.9	21.1	0.5	6.8	1.0	1.9	0.4	61.0	6.4	8.2	14.1	0.0	6.8	0.2	3.3
30	5	CA	M	22.2	17.7	14.8	41.6	0.0	1.0	2.4	0.0	0.4	25.8	14.4	33.5	21.8	0.0	1.7	2.8	0.0
31	5	CA	M	27.0	23.0	7.5	37.0	0.3	2.5	2.2	0.3	0.2	20.9	12.9	28.7	34.7	0.0	0.9	1.2	0.7
32	5	CA	M	16.0	19.9	14.5	46.1	0.0	2.1	1.2	0.0	0.1	8.1	12.1	34.1	39.2	0.4	3.4	2.5	0.2
33	12	CA	M	62.6	14.9	3.3	7.0	0.3	2.0	7.8	1.1	1.0	21.9	9.1	6.3	10.9	0.0	13.6	26.1	12.1
34	12	CA	M	78.0	9.2	1.6	7.5	0.0	3.3	0.0	0.1	0.2	32.3	18.9	18.8	14.9	0.0	8.7	3.6	2.8
35	12	CA	M	46.6	16.0	4.1	19.9	0.9	5.2	0.9	6.1	0.3	14.0	6.9	20.3	30.7	0.1	10.0	0.7	17.3
36	12	CA	M	13.5	20.7	7.0	51.2	0.2	6.1	1.0	0.0	0.2	3.9	9.4	32.3	42.5	0.1	8.2	3.7	0.0
37	9	W	M	87.8	4.5	0.0	0.4	0.0	0.0	0.3	6.9	0.0	27.4	6.4	1.0	1.0	0.0	0.3	1.5	62.5
38	9	W	M	48.5	8.2	1.0	4.3	0.0	0.1	0.3	37.3	0.3	18.8	5.9	0.2	3.3	0.0	0.3	0.4	71.0
39	9	W	M	14.6	14.7	0.0	6.5	0.0	0.6	0.5	62.0	1.1	5.7	2.9	0.0	0.7	0.0	0.1	0.1	90.5
40	9	W	M	77.6	7.0	0.4	1.6	0.1	11.7	0.6	1.0	0.0	27.6	6.4	2.1	14.1	0.7	21.3	1.4	26.3
41	9	W	M	91.1	2.6	0.0	0.8	0.0	0.8	0.0	4.7	0.0	37.9	7.2	4.0	8.1	0.2	6.8	0.1	35.7
42	9	W	M	98.0	1.4	0.0	0.0	0.0	0.0	0.0	0.5	0.0	34.4	8.0	3.7	8.7	0.1	4.8	1.9	38.5
43	12	CA	M	20.2	26.6	14.0	32.6	0.0	3.3	1.5	0.9	0.9	4.0	8.2	41.6	34.6	0.0	7.3	3.1	1.3
44	12	CA	M	30.0	29.6	11.3	24.2	0.3	2.9	0.9	0.4	0.5	14.2	20.4	28.9	28.1	0.1	4.6	1.1	2.6
45	9	W	H	78.4	6.1	0.4	3.5	0.1	8.1	0.1	2.9	0.5	54.9	4.7	1.9	17.5	0.1	5.7	0.3	14.9
46	9	W	H	83.0	5.4	0.1	2.3	0.0	4.7	0.0	4.6	0.0	39.4	6.0	3.4	1.7	1.1	21.4	0.0	26.8
47	9	W	H	98.3	0.9	0.4	0.1	0.0	0.1	0.0	0.2	0.0	47.4	5.4	7.7	13.3	0.0	5.9	0.0	20.2
48	9	W	H	94.2	2.5	0.1	0.6	0.0	1.4	0.3	1.0	0.0	78.1	2.8	3.9	0.3	0.0	1.2	0.1	13.6
49	8	MW	H	81.2	6.8	1.0	8.8	0.0	1.5	0.4	0.1	0.4	20.2	15.6	24.6	23.5	0.8	5.0	4.4	5.8
50	8	MW	H	26.1	25.3	6.4	38.2	0.0	3.0	0.9	0.1	0.0	13.8	15.3	19.5	45.4	0.0	3.3	1.4	1.4
51	8	MW	H	99.2	0.4	0.0	0.3	0.0	0.0	0.0	0.1	0.0	57.7	2.9	5.2	12.7	0.0	6.1	0.6	14.8
52	3	NA	H	14.7	15.1	6.0	54.8	0.0	4.7	3.5	0.6	0.6	11.2	13.1	14.3	47.6	0.0	7.6	6.0	0.2
53	3	NA	H	16.2	20.7	5.3	38.2	1.4	14.3	2.4	0.9	0.7	8.9	12.2	14.9	41.2	0.4	16.4	3.1	2.9
54	3	NA	H	22.9	11.2	10.1	25.0	0.4	7.6	1.9	19.5	1.3	11.2	5.9	14.4	24.5	0.0	8.5	1.1	34.4
55	3	NA	H	25.0	17.8	9.6	32.1	0.1	4.9	0.2	9.8	0.4	21.2	9.2	18.9	21.4	0.3	6.4	0.0	22.6
56	3	NA	H	29.7	18.8	3.9	26.2	0.0	20.9	0.4	0.1	0.0	20.6	12.2	8.3	14.1	0.1	37.1	7.2	0.4
57	3	NA	H	25.9	15.6	11.4	34.3	0.0	8.9	2.7	0.9	0.2	18.6	16.1	20.3	31.8	0.0	3.9	1.2	8.1
58	3	NA	H	29.9	25.0	2.9	33.6	0.6	4.8	1.8	1.3	0.1	20.3	13.1	14.6	37.4	0.0	12.6	1.3	0.7
59	3	NA	H	29.2	16.6	3.5	24.3	0.5	23.4	1.3	0.8	0.4	18.0	11.3	9.3	24.6	0.0	20.8	8.6	7.4
60	3	NA	H	44.0	16.7	6.2	28.1	0.4	3.5	0.2	1.0	0.0	36.5	10.5	18.3	24.7	0.4	7.3	0.0	2.3

61	3	NA	H	55.6	10.3	9.7	17.3	0.6	3.5	1.4	1.6	0.0	51.3	12.5	14.0	6.0	0.2	7.4	1.7	7.0
62	3	NA	H	35.6	17.9	15.6	24.6	0.0	4.2	1.4	0.5	0.1	29.0	16.2	19.7	23.6	0.0	7.7	0.8	3.0
63	3	NA	H	28.1	20.8	9.5	37.5	0.3	3.6	0.0	0.0	0.1	19.8	11.5	33.9	22.0	0.3	10.8	1.6	0.0
64	4	CA	H	16.2	17.1	2.7	35.3	2.1	16.6	8.9	0.1	1.1	7.5	10.8	11.0	39.7	0.8	22.5	6.3	1.4
65	7	CKY	H	28.1	17.5	5.9	38.6	0.5	5.6	3.3	0.2	0.4	25.4	11.9	20.2	24.0	0.0	15.4	2.1	1.0
66	7	CKY	H	32.2	17.7	2.4	28.1	0.9	16.9	1.4	0.1	0.4	6.5	9.0	7.9	33.1	0.6	40.7	1.8	0.4
67	4	CA	H	90.2	3.3	0.4	1.1	0.0	0.3	0.5	3.9	0.3	83.4	2.4	4.6	1.1	0.0	0.0	0.2	8.3
68	4	CA	H	75.1	7.1	1.8	11.9	0.0	3.3	0.7	0.0	0.1	71.9	11.3	5.5	10.4	0.0	0.8	0.2	0.0
69	4	CA	H	33.5	19.1	2.2	10.5	3.7	16.8	12.6	0.4	1.3	28.4	15.2	17.4	14.5	1.5	16.7	5.3	1.1
70	4	CA	H	37.2	12.8	11.8	13.2	0.6	23.3	0.8	0.1	0.2	17.8	12.7	24.7	15.7	6.0	22.6	0.5	0.1
71	4	CA	H	90.4	6.9	0.1	1.0	0.0	1.2	0.0	0.3	0.0	65.5	9.0	7.0	6.4	0.0	9.1	0.3	2.7
72	4	CA	H	23.1	19.4	5.7	43.0	0.1	6.3	1.6	0.2	0.6	8.8	13.7	19.9	42.4	0.3	10.3	3.1	1.4
73	4	CA	H	11.9	18.9	9.1	45.4	0.1	10.5	3.0	0.7	0.5	10.8	9.6	21.5	39.0	0.1	14.9	0.7	3.3
74	4	CA	H	14.0	21.2	10.6	46.8	0.5	4.9	1.0	0.8	0.2	9.0	12.7	31.2	35.0	0.1	9.7	0.3	2.0
75	4	CA	H	17.0	20.4	6.2	43.2	0.3	10.6	1.1	1.0	0.3	13.2	15.6	21.8	30.0	0.0	14.5	0.2	4.7
76	9	W	H	45.5	11.8	6.9	16.8	1.1	14.3	1.2	1.9	0.4	36.9	6.2	13.1	21.0	0.0	12.9	0.3	9.5
77	9	W	H	38.3	19.2	2.4	23.1	0.5	13.9	0.6	2.0	0.1	12.2	8.3	2.1	25.2	1.2	34.7	2.6	13.8
78	9	W	H	83.2	8.4	0.0	1.8	0.3	0.2	0.3	5.7	0.1	24.9	6.8	0.7	12.1	0.2	3.7	0.2	51.6
79	9	W	H	76.5	7.2	1.3	5.9	0.0	3.7	0.3	5.1	0.0	44.4	14.9	8.3	7.5	0.0	4.5	0.0	20.3
80	9	W	H	94.9	1.3	0.0	1.3	0.0	0.6	0.0	1.9	0.0	43.7	6.1	0.3	2.6	0.3	8.5	0.3	38.2
81	9	W	H	68.2	18.0	0.1	2.7	0.0	7.4	0.0	3.3	0.3	43.6	10.0	1.9	2.4	0.0	3.3	0.0	38.8
82	4	CA	H	47.5	16.7	3.3	18.9	0.3	6.1	1.7	5.3	0.1	15.7	8.9	18.1	25.9	0.0	11.6	0.5	19.5
83	7	CKY	H	15.3	26.4	4.8	48.6	0.0	2.8	0.7	0.4	1.0	9.9	10.4	9.1	54.7	0.0	11.1	4.0	0.8
84	7	CKY	H	17.9	16.6	4.4	42.5	2.2	14.6	1.2	0.3	0.4	6.6	16.4	9.6	42.3	0.6	23.7	0.5	0.2
85	7	CKY	H	17.3	20.1	5.6	45.6	0.2	5.5	4.1	0.8	0.8	7.7	10.7	24.6	39.2	0.0	14.2	2.6	1.0
86	7	CKY	H	7.0	11.7	1.8	14.8	2.4	61.7	0.0	0.3	0.3	0.7	5.0	2.5	21.1	0.5	69.5	0.6	0.0
87	7	CKY	H	32.8	24.6	5.9	26.8	0.2	3.3	5.0	0.8	0.7	18.4	10.4	14.6	37.7	0.6	8.9	9.3	0.0
88	7	CKY	H	10.7	17.4	2.6	46.1	0.3	21.0	0.9	0.8	0.4	3.7	9.7	9.2	56.8	0.1	17.4	0.5	2.5
89	7	CKY	H	30.7	20.5	11.1	31.2	0.0	3.0	2.5	1.0	0.1	19.1	9.4	35.4	29.8	0.0	2.7	0.8	2.7
90	7	CKY	H	69.8	11.4	1.3	8.5	0.8	6.2	0.4	1.1	0.5	13.6	6.1	19.5	39.8	0.9	12.4	0.8	7.0
91	11	AL	H	91.5	2.1	0.2	3.8	0.0	1.2	1.0	0.2	0.0	26.5	9.2	21.5	12.5	0.0	11.6	4.9	13.7
92	11	AL	H	69.8	11.8	1.1	11.3	0.0	1.2	0.7	3.8	0.4	18.5	11.7	18.6	13.3	0.0	9.3	2.5	26.0

93	11	AL	H	72.3	7.2	1.2	12.3	0.0	5.8	0.0	1.0	0.1	19.0	14.2	21.4	22.3	0.3	19.3	0.0	3.6
94	11	AL	H	60.4	9.1	0.6	13.6	0.7	10.9	2.6	2.0	0.1	7.8	10.1	3.9	22.5	0.3	13.0	3.5	38.9
95	11	AL	H	94.5	1.2	0.9	1.2	0.0	0.3	1.3	0.5	0.0	31.3	9.5	22.1	10.4	0.0	11.6	2.4	12.7
96	11	AL	H	95.8	0.7	0.0	0.7	0.0	2.4	0.0	0.4	0.0	51.2	5.1	2.2	12.9	0.0	12.3	0.0	16.3
97	11	AL	H	97.4	0.5	0.0	0.4	0.0	0.4	0.0	1.2	0.0	23.4	11.0	4.4	15.2	0.8	7.3	5.9	32.0
98	11	AL	H	81.7	5.5	0.0	1.3	0.0	10.8	0.0	0.6	0.0	28.2	7.2	4.0	2.8	0.8	23.7	0.0	33.4
99	11	AL	H	97.9	0.1	0.4	0.0	0.0	0.8	0.7	0.1	0.0	26.8	9.2	13.5	11.9	0.3	11.5	2.8	24.2
100	7	CKY	H	19.3	21.8	9.0	43.1	0.0	3.6	2.5	0.3	0.4	7.2	10.9	33.4	36.5	0.1	9.4	2.2	0.2
101	7	CKY	H	52.1	9.2	4.2	24.8	0.7	4.9	3.3	0.5	0.4	50.2	11.0	10.8	15.7	0.0	6.9	3.9	1.5
102	3	NA	H	51.1	16.2	4.4	19.4	0.1	2.3	1.5	4.4	0.7	44.4	11.5	9.3	14.3	0.0	4.9	1.8	13.8
103	7	CKY	H	9.8	12.6	8.7	56.4	0.3	4.4	3.7	0.0	4.1	4.0	8.0	31.1	42.7	0.4	9.4	4.4	0.0

Appendix B: Particle mineralogy and size distributions per sample

Table B1. Mineralogical distributions based on particle counts and masses for each **historical sample** per mine region/MSHA district. Mine region: NA=northern Appalachia, CA=central Appalachia, CKY=central Kentucky, MW=mid-west, W=west, AL=Alabama; mineralogical distribution: C=carbonaceous, MC=mixed-carbonaceous, ASK=kaolinite-like silicates, ASO=other aluminosilicates, SLO=other silicates, S=silica, M=heavy minerals, CB=carbonates, O=other. Sampling location are in parenthesis. (LW=longwall mining, CM=continuous miner, P=production, B=bolter).

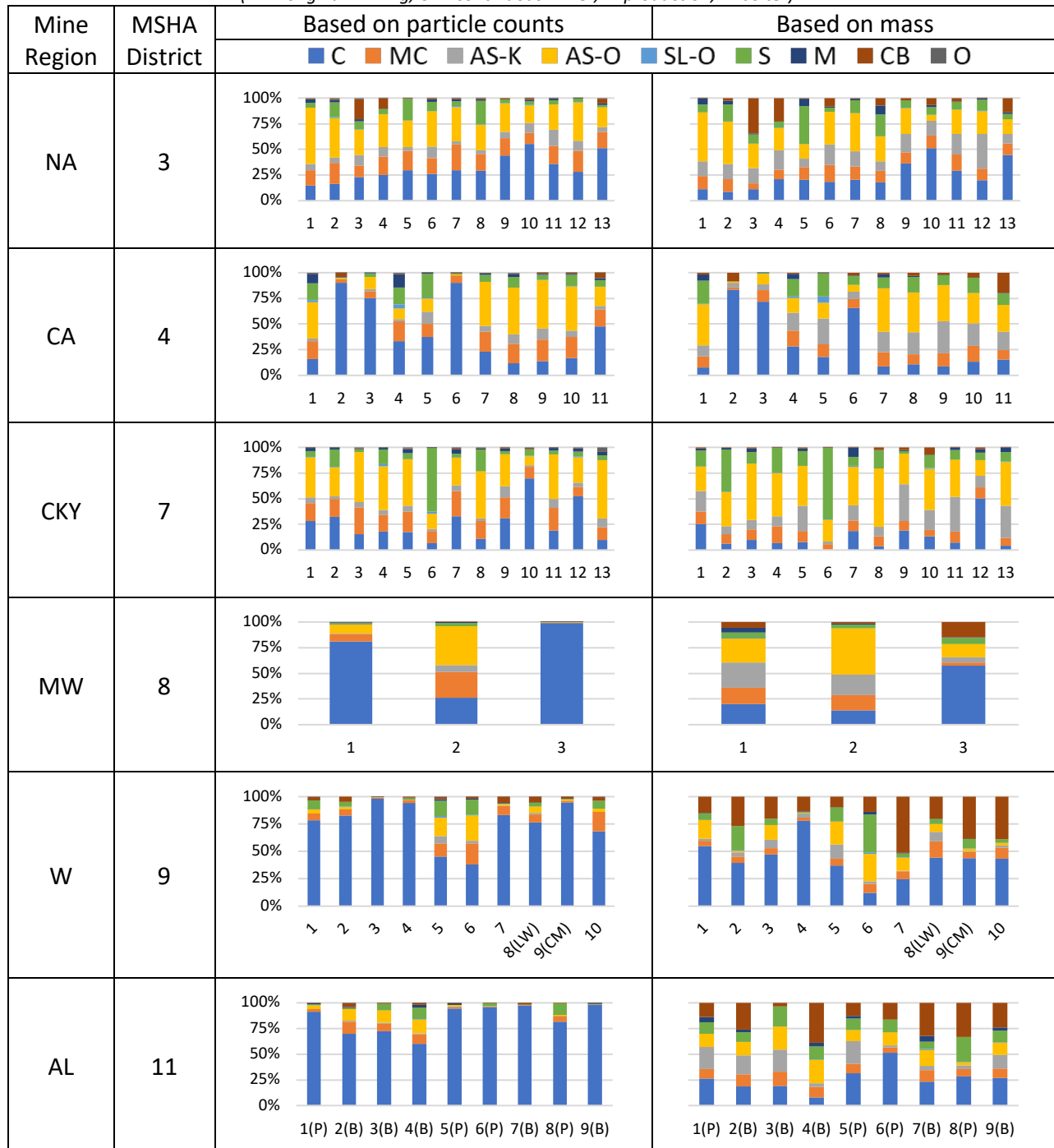


Table B2. Mineralogical distributions based on particle counts and masses for each **modern sample** per mine region/MSHA district. Mine region: NA=northern Appalachia, CA=central Appalachia, MW=mid-west, W=west; mineralogical distribution: C=carbonaceous, MC=mixed-carbonaceous, ASK=kaolinite-like silicates, ASO=other aluminosilicates, SLO=other silicates, S=silica, M=heavy minerals, CB=carbonates, O=other. Sampling location are in parenthesis. (B=bolter, P=production, R=return, I=intake, F=feeder).

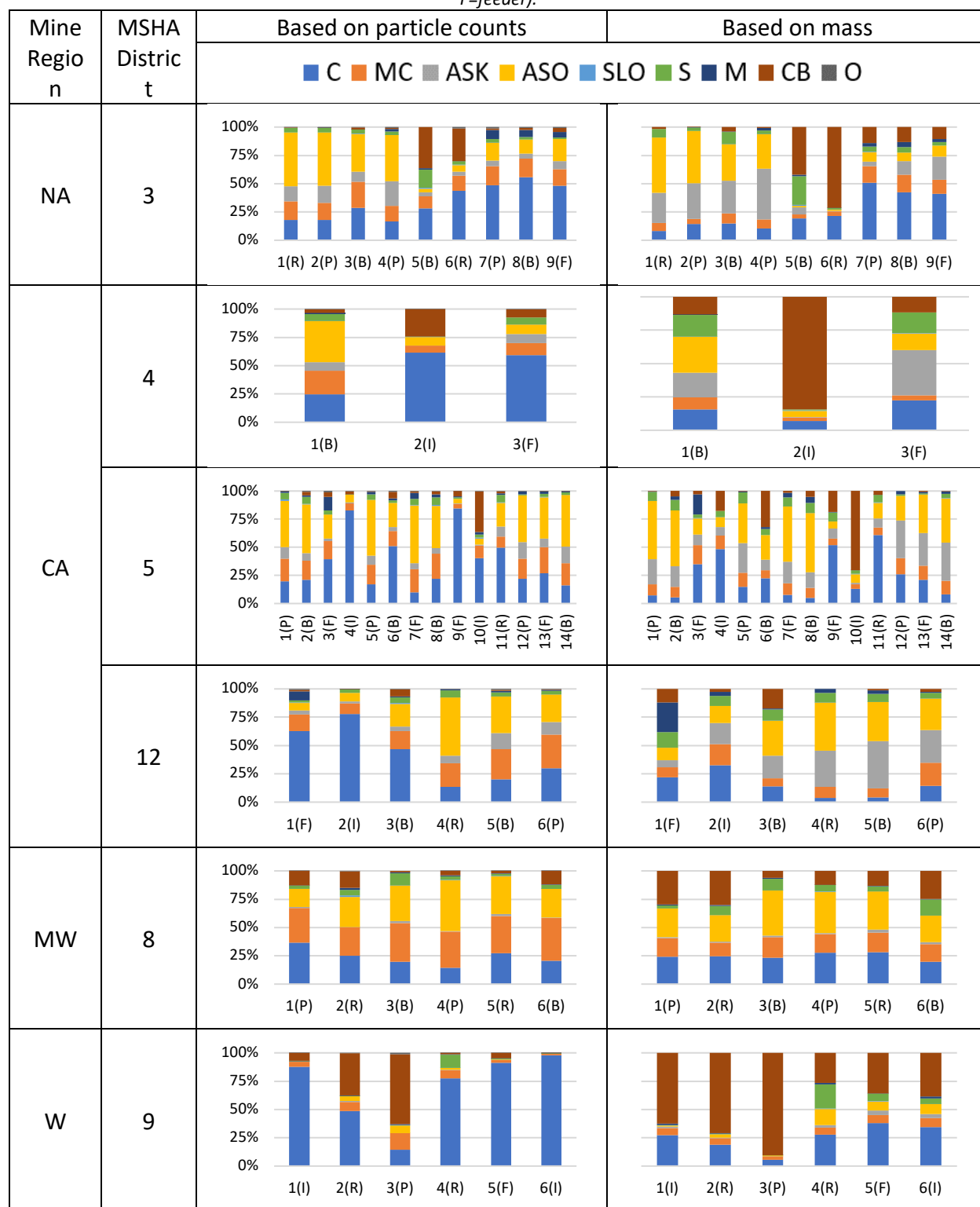


Table B3. Mineralogical distributions (**without carbonates (i.e., CB)**) based on particle counts and masses for each **historical sample** per mine region/MSHA district. Mine region: NA=northern Appalachia, CA=central Appalachia, CKY=central Kentucky, MW=mid-west, W=west, AL=Alabama; mineralogical distribution: C=carbonaceous, MC=mixed-carbonaceous, ASK= kaolinite-like silicates, ASO=other aluminosilicates, SLO=other silicates, S=silica, M=heavy minerals, O=other. (LW=longwall mining, CM=continuous miner, P=production, B=bolter).

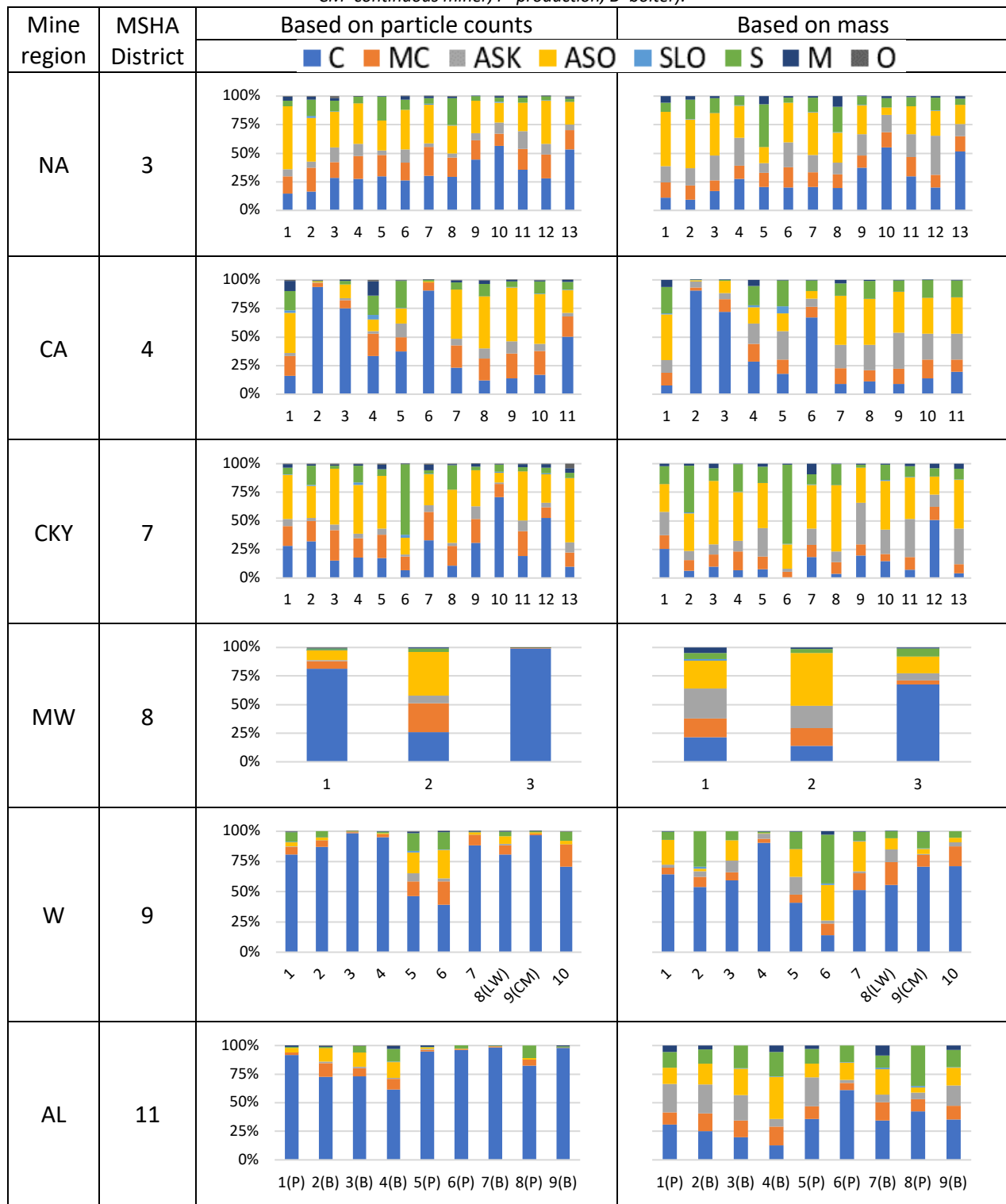


Table B4. Mineralogical distributions (without carbonates (i.e., CB)) based on particle counts and masses for each modern sample per mine region/MSHA district. Mine region: NA=northern Appalachia, CA=central Appalachia, MW=mid-west, W=west; mineralogical distribution: C=carbonaceous, MC=mixed-carbonaceous, kaolinite-like silicates, ASO=other aluminosilicates, SLO=other silicates, S=silica, M=heavy minerals, O=other. Sampling location are in parenthesis. (B=bolter, P=production, R=return, I=intake, F=feeder).

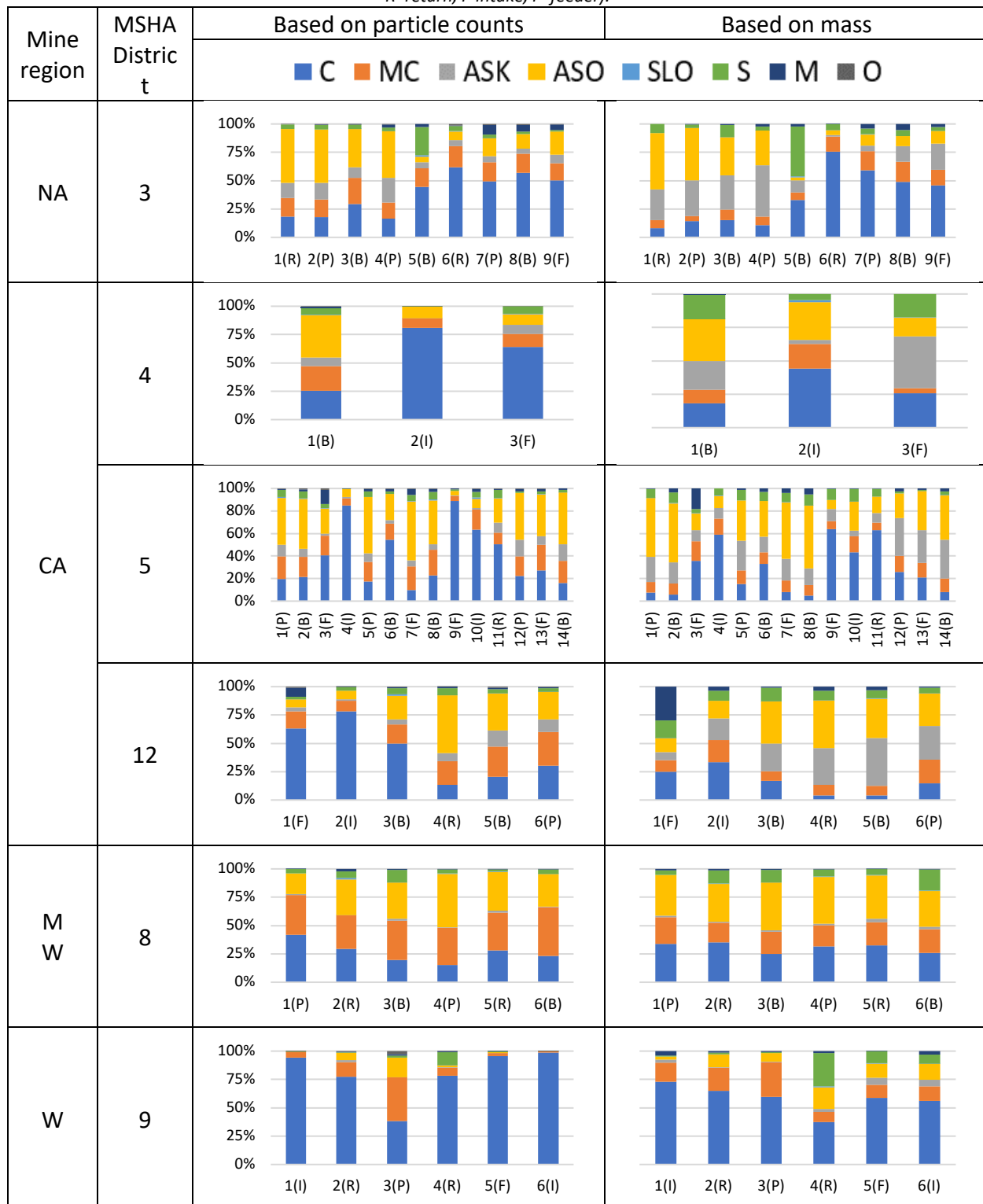


Table B5. Cumulative particle size distributions for each historical sample per mine region/MSHA district. Where known definitively, the sampling location is indicated (LW=longwall mining, CM=continuous miner, P=production, B=bolter).

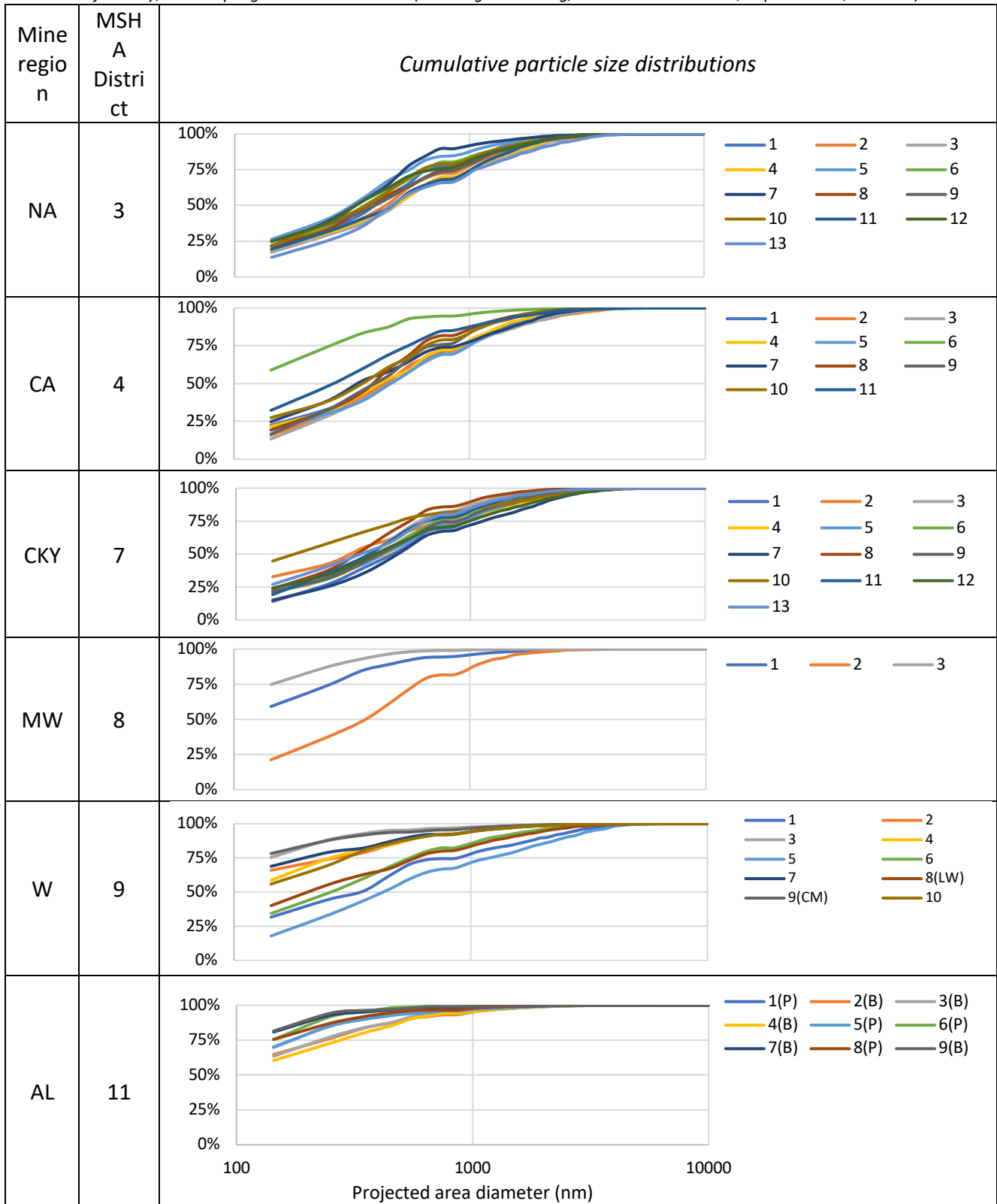
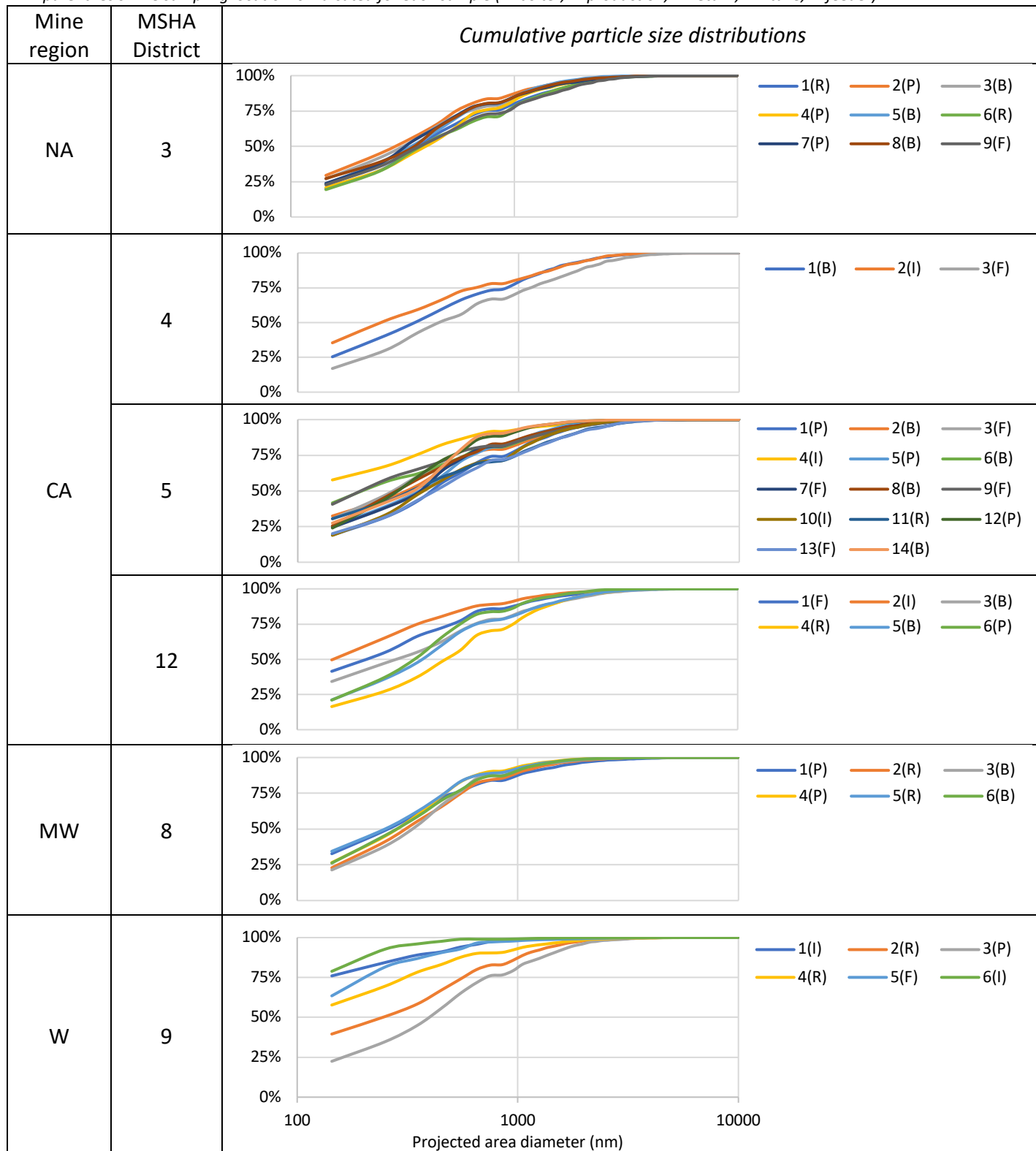


Table B6. Cumulative particle size distributions for each **modern sample** per mine region/MSHA district. Sampling location are in parenthesis. The sampling location is indicated for each sample (B=bolter, P=production, R=return, I=intake, F=feeder).



Appendix C: Example SEM-EDX images

Figure C1. SEM-EDX images from northern Appalachia (MSHA district 3) with elemental maps. Al is red, Si is green. Images were captured at 5kV and 5000× magnification.

NA (MSHA District 3)

Modern Samples

Historical Samples

Sample 3 (B)

Sample 2

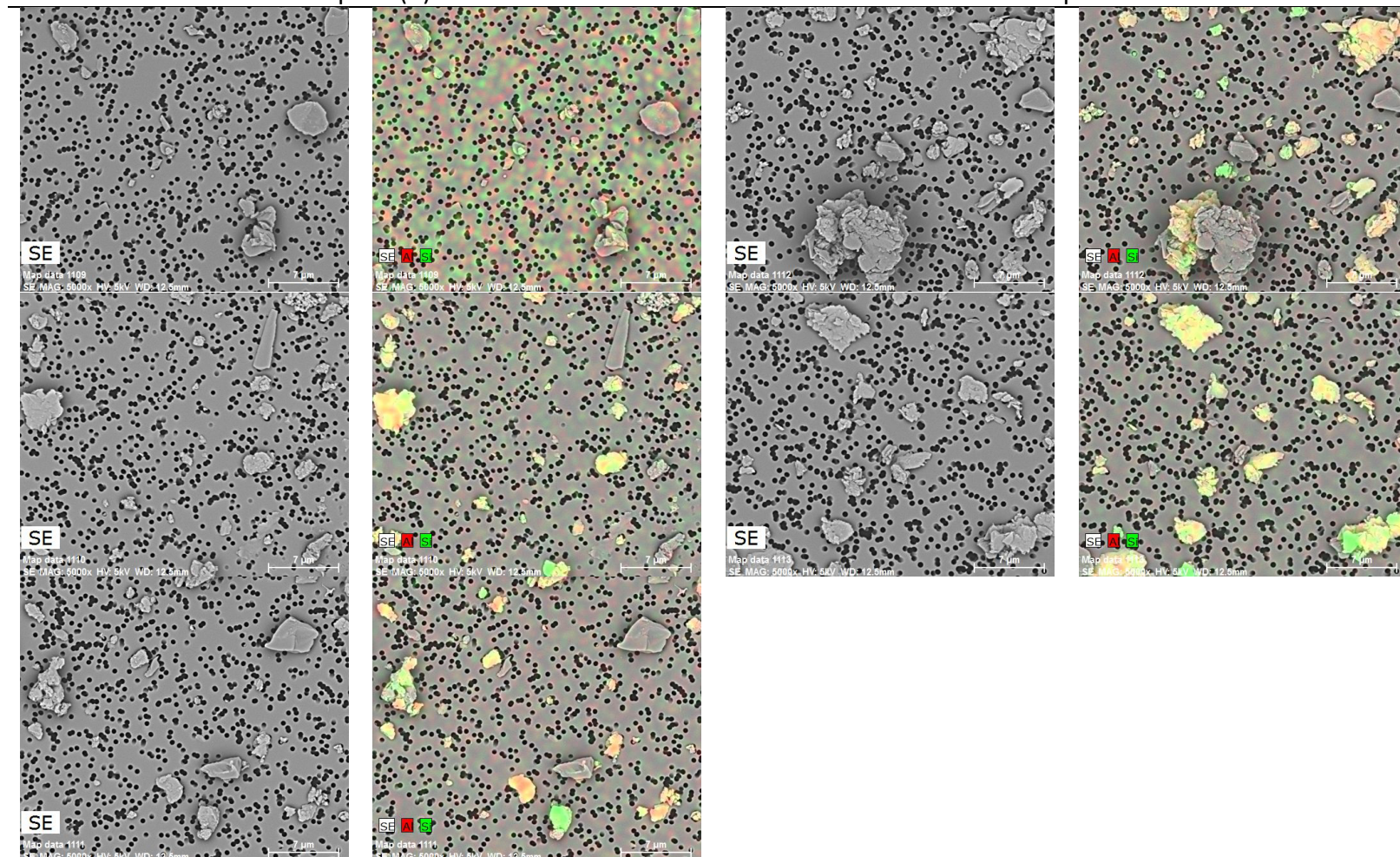


Figure C2. SEM-EDX images from **central Appalachia (MSHA district 4)** with elemental maps. Al is red, Si is green. Images were captured at 5kV and 5000× magnification.

CA (MSHA District 4)

Modern Samples

Sample 1 (B)

Historical Samples

Sample 2

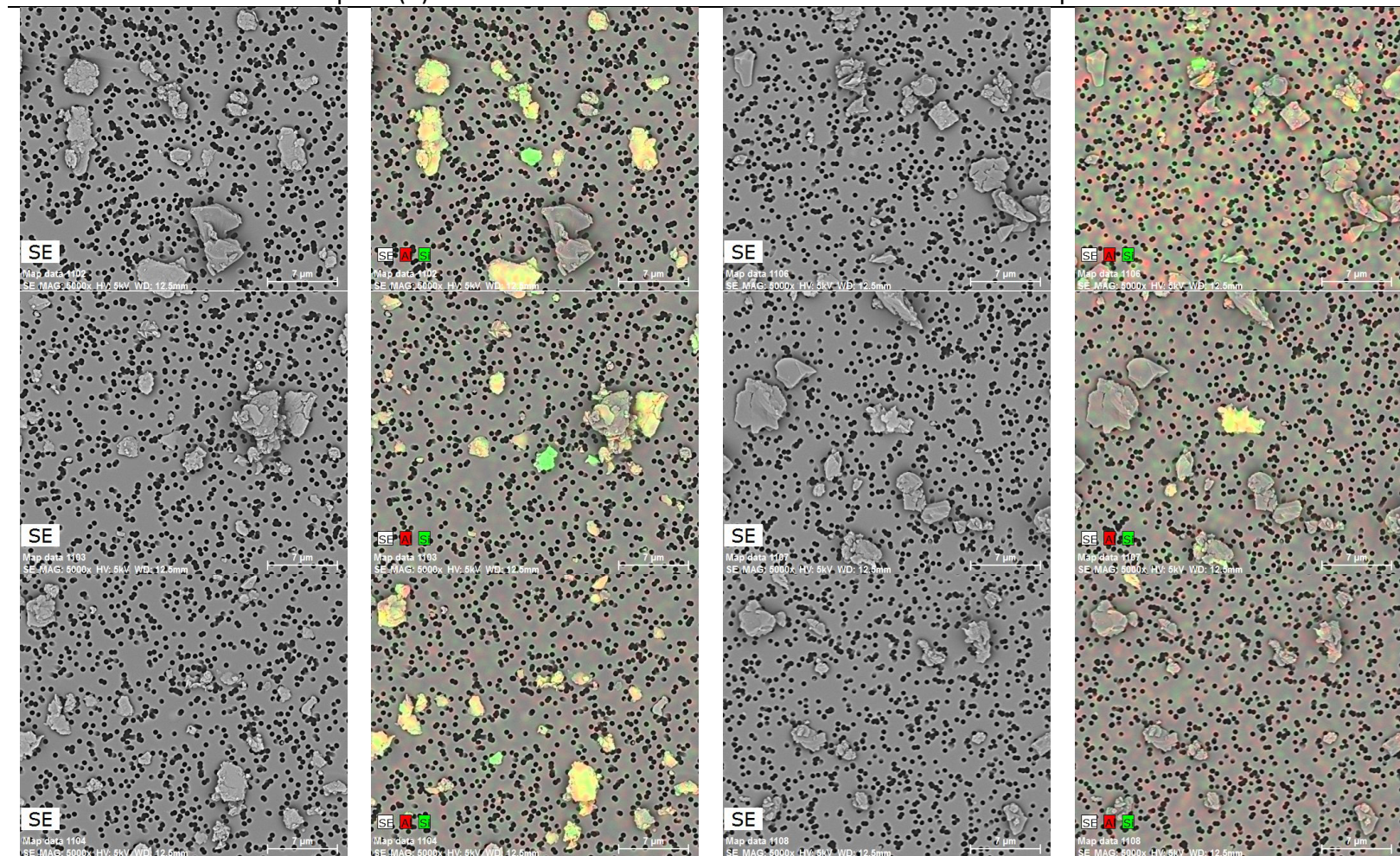


Figure C3. SEM-EDX images from **Mid-west (MSHA district 8)** with elemental maps. Al is red, Si is green. Images were captured at 5kV and 5000× magnification.

MW (MSHA District 8)

Modern Samples

Sample 4 (P)

Historical Samples

Sample 2

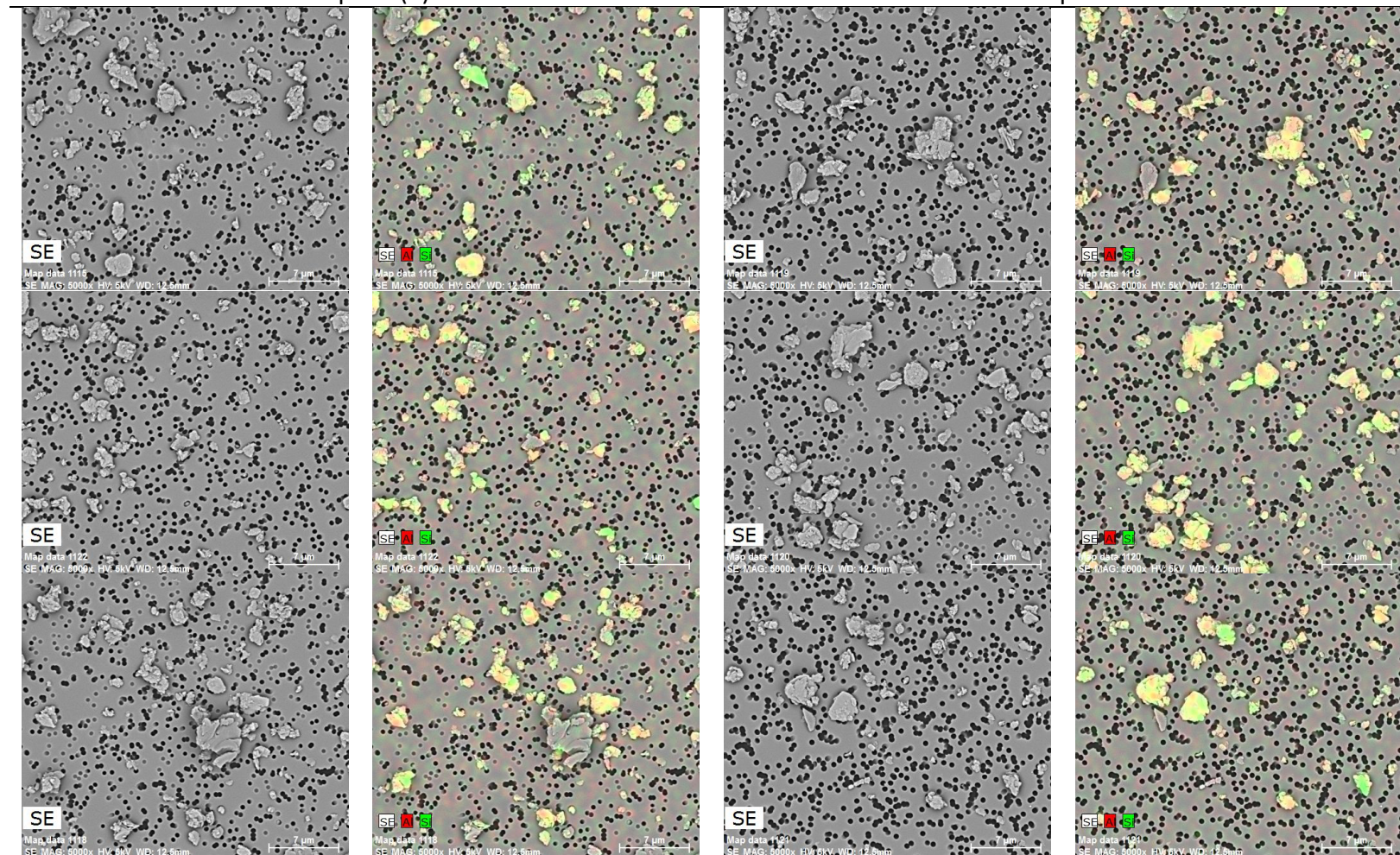


Figure C4. SEM-EDX images from **West (MSHA district 9)** with elemental maps. Al is red, Si is green. Images were captured at 5kV and 5000× magnification.

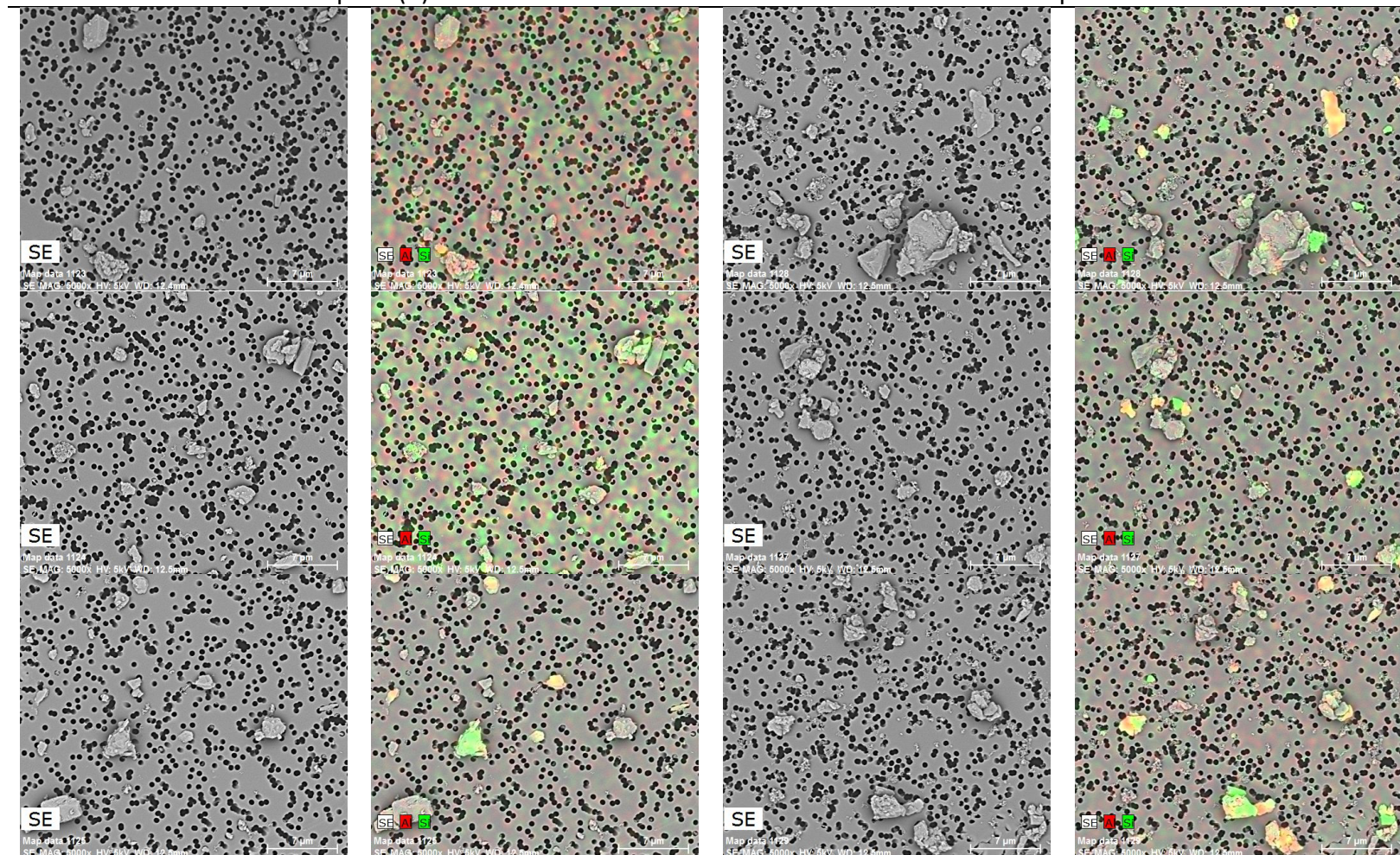
W (MSHA District 9)

Modern Samples

Sample 2 (R)

Historical Samples

Sample 2



Appendix D: Assessment of FTIR data quality

Key limitations for the FTIR analysis conducted for this project include:

- (1) Since FTIR is a mass-based method, sufficient analyte mass (i.e., quartz, kaolinite, or calcite) is required in the sample to achieve accurate results. This means that samples with relatively low total sample mass and/or analyte % might exhibit results below the limit of detection (LOD) or limit of quantification (LOQ). Samples with low mass are also more prone to errors in weight measurements, which can impact estimates of analyte % values. For the analysis included in this report, we have considered 100 µg as a “low sample mass” threshold.
- (2) Analyte mass in a sample is estimated by translating the FTIR spectral data (i.e., integrated peak area for some characteristic wavelength range for each analyte) obtained on a small (6-mm) circular area in the center of a sample filter to the entire filter area using a model of the dust deposition pattern; then mass % is computed using the total sample mass. The dust deposition pattern is a characteristic of the sampling cassette and dust concentration in the sampling environment. For the modern dust samples being examined on this project (collected in 2-piece styrene cassettes), we know the deposition pattern should be fairly consistent and we have derived a model for translating the FTIR spectra to analyte mass on the filter (i.e., based on work by Miller et al., 2013 and described in Pokhrel et al., 2022). However, for the historical samples (collected in MSA cassettes), the deposition pattern is known to be less predictable (also based on Miller et al., 2013) and we identified several possible models for FTIR spectra-to-analyte mass translation. One such model is incorporated into the current version of the *FAST* software that NIOSH has developed for direct-on-filter silica analysis in respirable coal mine dust samples, and we have determined it should give “high end” estimates of the analytes of interest here. Another model can be derived from the Miller et al. (2013) work, and we have determined it should give “low end” estimates. For the analysis included in this report, we employed both of these models.
- (3) Following from the above two points, it should also be acknowledged that the historical samples available for this project were 17-19 years old at the time of our FTIR work. The effects of sample/background filter aging on FTIR analysis are unknown, as are the effects on potential for sample loss.

To assess these limitations and quality of the FTIR data collected for this project, some comparisons can be made between the FTIR and SEM-EDX data. Figure D1 shows the difference between mass % estimates of quartz, kaolinite and calcite derived from FTIR analysis and estimates of silica, kaolinite-like silicates, and carbonates derived from SEM-EDX data for the modern samples as a function of sample mass. (Only samples with FTIR results > LOD are shown; LOD is about 5 µg for quartz, 5 µg for kaolinite, and 3 µg for calcite.) The effect of sample mass is especially evident for the kaolinite estimates. There is more disagreement in the SEM-EDX and FTIR results for relatively low-mass samples, with the FTIR tending to predict much more kaolinite

than the SEM-EDX. There is also significant disagreement between the SEM-EDX carbonates and FTIR calcite for several samples—though this seems less related to sample mass and is probably due to the presence of non-calcite carbonates in some samples (i.e., such that the FTIR appears to underpredict calcite relative to SEM-EDX carbonates). Agreement is good for the small number of samples for which FTIR silica was > LOD.

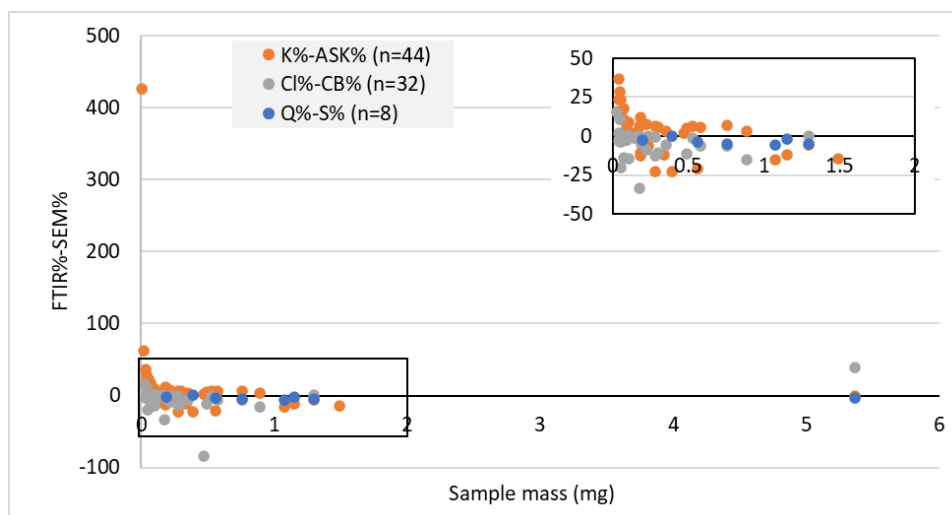


Figure D1. Difference between FTIR-derived mass % of quartz, kaolinite, or calcite and SEM-EDX derived mass % of silica, kaolinite-like silicates, or carbonates for modern dust samples as a function of sample mass. The larger plot shows all data points and the inset provides a higher resolution view of majority of points clustered together.

Figure D2 shows the correlations between the FTIR and SEM-EDX data for each of the three analyte pairs for the modern samples, with and without excluding low-mass samples (< 100 μg). For the calcite/carbonates, there is a clear correlation between the FTIR and SEM-EDX derived results, though they do not match perfectly. This is to be expected since the SEM-EDX data is related to all calcium and magnesium carbonates observed in the samples, whereas the FTIR is specific to calcite. Moreover, the SEM-EDX data is particle based, and some assumptions are made to translate number % data to mass % estimates. Per the above discussion of Figure D1, application of a low mass threshold does not significantly impact the correlation.

For the kaolinite estimates, the effect of sample mass on the FTIR results is again evident in Figure D2 (i.e., virtually no correlation exists when low-mass samples are considered). After excluding low mass samples, a correlation is clear, but the linear trendline slope between FTIR and SEM-EDX mass % estimates is relatively low. This could simply be due to the fact that the SEM-EDX classification criteria were developed for kaolinite-like silicates, meaning they stoichiometrically similar amounts of Al and Si; however, the FTIR method should only measure kaolinite.

For silica/quartz, just eight of the modern had FTIR results > LOD (and these same samples also had total dust weight > 100 μg). While only a very weak correlation can be seen between the SEM-EDX and FTIR derived estimates, this is because the range of silica/quartz percentages covered by these samples is quite small. Indeed, the two methods disagreed by no more than +/- 6%.

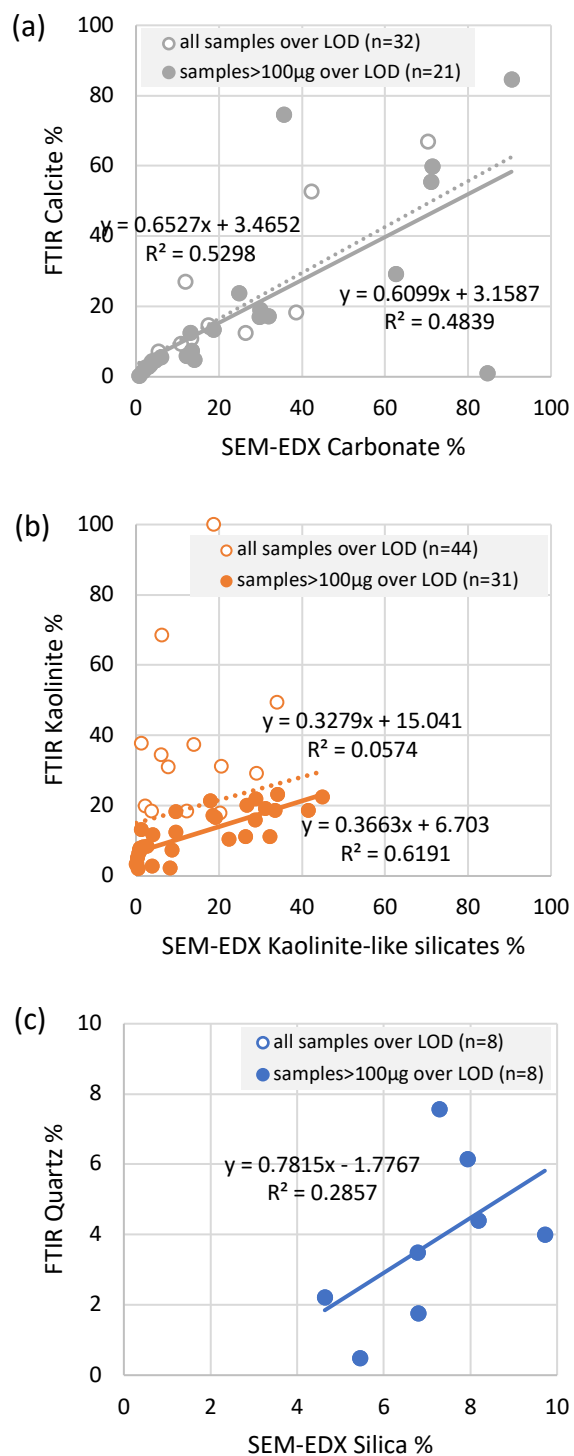


Figure D2. FTIR-derived mass % of (a) calcite, (b) kaolinite or (c) quartz versus SEM-EDX derived mass % of (a) carbonates, (b) kaolinite-like silicates, or (c) silica for modern dust samples. The open points show all samples with available data to date; the solid points show samples with total mass > 100 µg.

Figure D3 is analogous to Figure D1 for the historical samples. (Again, only samples with FTIR results > LOD are shown.) Plot (a) shows the FTIR results using the FAST model to extrapolate the

mineral measurements from the filter center to the entire filter area, and plot (b) shows the FTIR results using the Miller et al. (2013) model. In both cases, most of the data points (FITR%-SEM%) are still in $\pm 25\%$ range, as was observed for the modern samples. However, for the historical samples, the scatter of data seems less dependent on sample mass. This might be related to differences in the dust deposition patterns characteristic of the MSA (historical) versus 2-piece (modern) sampling cassettes.

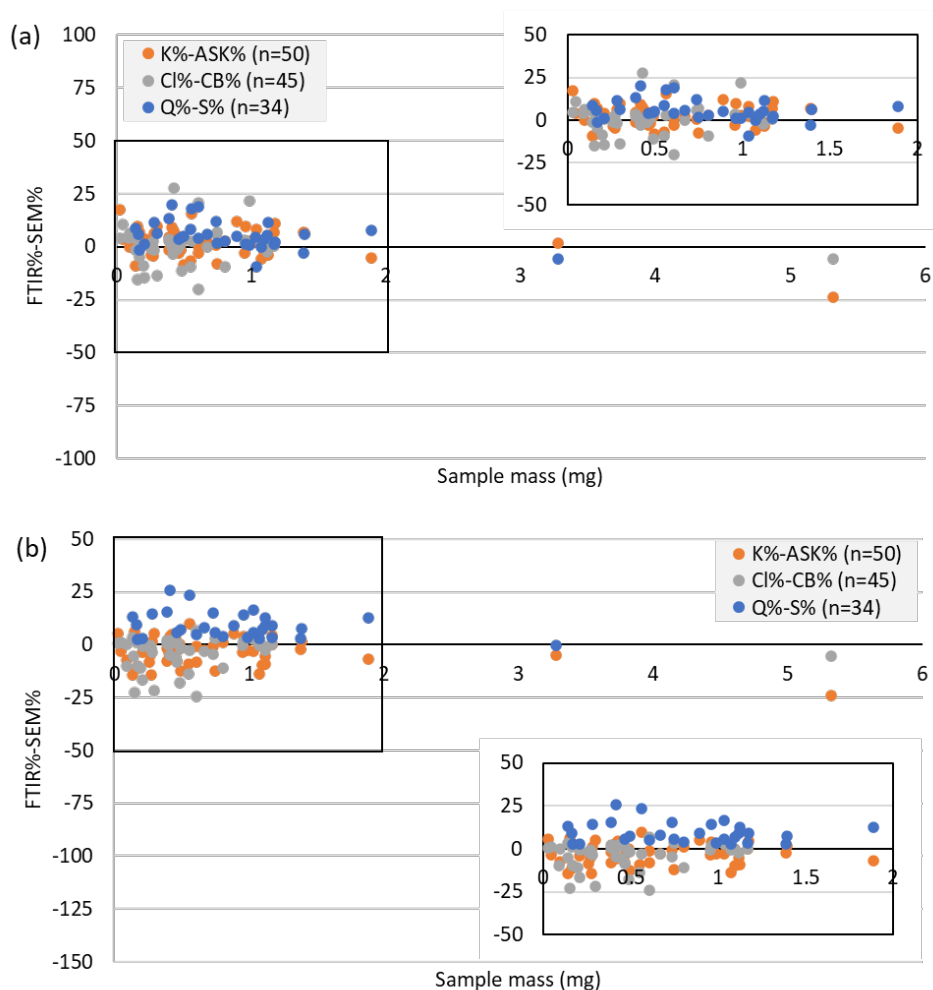


Figure D3. Difference between FTIR-derived mass % of quartz, kaolinite, or calcite and SEM-EDX derived mass % of silica, kaolinite-like silicates, or carbonates for historic dust samples as a function of sample mass. (a) FTIR results are based on FAST measurements, (b) FTIR results are based on equations from Miller et al. 2013. The larger plots show all data points and the insets provides a higher resolution view of majority of points clustered together.

Figure D4 is analogous to Figure D2 for the historical samples. The plots on the left present the FTIR results based on FAST model, and the plots on the left are based on the Miller et al. (2013) model. Similar to the modern samples, the FTIR and SEM-EDX results showed a clear correlation for calcite/carbonates. The correlation for kaolinite-like silicates was not as good, but, like for the modern samples, the trendline slope suggests that the SEM-EDX kaolinite-like class includes particles other than kaolinite. For the silica/quartz results for historical samples, there is still

scatter in the data like observed for the modern samples; however, a few relatively high-content samples served to improve the correlation coefficient.

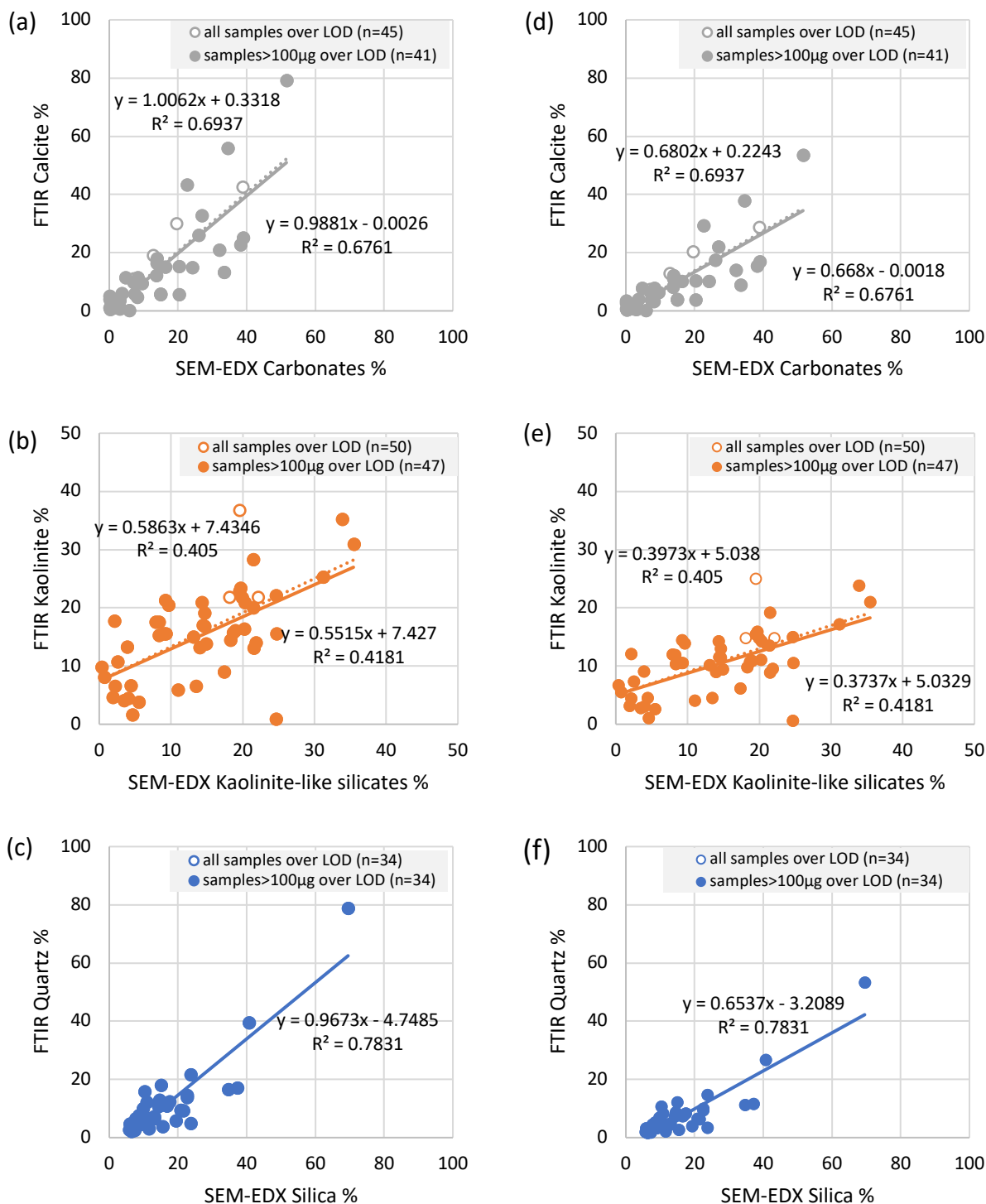


Figure D4. FTIR-derived mass % of (a, d) calcite, (b, e) kaolinite or (c, f) quartz versus SEM-EDX derived mass % of (a, d) carbonates, (b, e) kaolinite-like silicates, or (c, f) silica for modern dust samples. (a, b, c) FTIR results are based on FAST measurements, (d, e, f) FTIR results are based on equations from Miller et al. 2013. The open points show all samples; the solid points show samples with total mass > 100 μ g.

Figure D4 indicates the *FAST* model, as opposed to the Miller et al. model, yields a better match between the FTIR results and those derived from the SEM-EDX analysis for the historical samples. For example, the *FAST* model yielded a trendline slope of nearly 1.0 for both the calcite/carbonates and quartz/silica results. However, the Miller et al. model yielded results that are more appropriate for the purpose of comparing the FTIR results between the historical and modern samples. This is because for all three minerals, the Miller et al. trendlines are more similar to those observed for the modern samples (Figure D2).